

Distinguishing Biotic and Abiotic Iron Oxidation at Low Temperatures

Brian St Clair,^{*,†,‡,§,||} Justin Pottenger,[†] Randall Debes,^{†,||} Kurt Hanselmann,[§] and Everett Shock^{†,||,⊥}

[†]Group Exploring Organic Processes in Geochemistry, Arizona State University, Tempe, Arizona 85287, United States

[‡]Environmental Life Sciences, Arizona State University, Tempe, Arizona 85287, United States

[§]Department of Earth Sciences, Swiss Federal Institute of Technology (ETH) Zurich, Zürich CH-8092, Switzerland

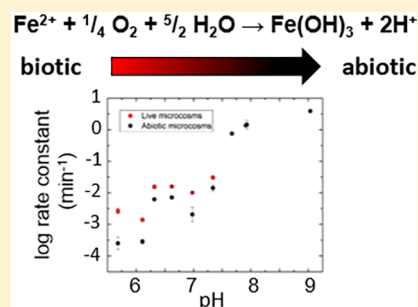
^{||}School of Earth & Space Exploration, Arizona State University, Tempe, Arizona 85287, United States

[⊥]School of Molecular Sciences, Arizona State University, Tempe, Arizona 85287, United States

Supporting Information

ABSTRACT: The rates of microbial and abiotic iron oxidation were determined in a variety of cold ($T = 9\text{--}12\text{ }^{\circ}\text{C}$), circumneutral ($\text{pH} = 5.5\text{--}9.0$) environments in the Swiss Alps. These habitats include iron–bicarbonate springs, iron–arsenic–bicarbonate springs, and alpine lakes. Rates of microbial iron oxidation were measured up to a pH of 7.4, with only abiotic processes detected at higher pH values. Iron oxidizing bacteria (FeOB) were responsible for 39–89% of the net oxidation rate at locations where biological iron oxidation was detected. Members of putative iron oxidizing genera, especially *Gallionella*, are abundant in systems where biological iron oxidation was measured. Geochemical sampling suites accompanying each experiment include field data (temperature, pH , conductivity, dissolved oxygen, and redox sensitive solutes), solute concentrations, and sediment composition. Dissolved inorganic carbon concentrations indicate that bicarbonate and carbonate are typically the most abundant anions in these systems. Speciation calculations reveal that ferrous iron typically exists as $\text{FeCO}_3(\text{aq})$, FeHCO_3^+ , $\text{FeSO}_4(\text{aq})$, or Fe^{2+} in these systems. The abundance of ferrous carbonate and bicarbonate species appears to lead to a dramatic increase in the abiotic rate of reaction compared to the rate expected from chemical oxidation in dilute solution. This approach, integrating geochemistry, rates, and community composition, reveals locations and geochemical conditions that permit microbial iron oxidation and locations where the abiotic rate is too fast for the biotic process to compete.

KEYWORDS: iron oxidizing bacteria, iron redox cycling, rate experiments, chemical speciation, metal carbonates, metal bicarbonates, *Gallionella*



1. INTRODUCTION

Iron oxidizing bacteria (FeOB) catalyze the reaction of $\text{Fe}(\text{II})$ with molecular oxygen to gain metabolic energy, generating ferric minerals as byproducts. An idealized reaction stoichiometry is $\text{Fe}^{2+} + (\frac{1}{4})\text{O}_2 + (\frac{5}{2})\text{H}_2\text{O} \rightarrow \text{Fe}(\text{OH})_3 + 2\text{H}^+$. Other $\text{Fe}(\text{II})$ couplings, such as nitrate-dependent oxidation¹ and photoferrotrophy,² have also been documented (and recently reviewed³). The present contribution focuses exclusively on oxidation via atmospheric or dissolved O_2 . Biological iron oxidation was previously documented in a wide variety of circumneutral habitats, including iron-rich springs,^{4,5} the arctic tundra,⁶ caves,⁷ ocean seeps,⁸ and other environments where reduced iron and atmospheric oxygen are out of equilibrium. In the present study, iron springs and iron-cycling lakes in the Swiss Alps, with greatly varying compositions, were studied to assess kinetics of microbial and abiotic iron oxidation across a wide range of low-temperature geochemical conditions.

In oxic circumneutral environments, abiotic $\text{Fe}(\text{II})$ oxidation can be extremely rapid. FeOB compete with the abiotic oxidation process for $\text{Fe}(\text{II})$, which requires quantification of

the relative contributions of FeOB and abiotic rates to place FeOB in their broader biogeochemical context. In situ rate measurements of oxidation attributable to FeOB in circumneutral environments are emerging.^{4,7,9,10} Using literature data, Emerson et al.¹¹ calculated that FeOB contributed an average of 45% of the net rate of $\text{Fe}(\text{II})$ oxidation. This result is based on a limited number of examples, however, and the reported range is from 28 to 75%.⁹ Rate measurements of FeOB in pure culture also show competition from abiotic processes.^{12–15} Recent studies have cataloged how geochemistry in circumneutral environments affects broader biogeochemical cycling of iron.^{15,16} A goal of the present study was to determine conditions where the abiotic $\text{Fe}(\text{II})$ oxidation rate is so fast that biology cannot compete at a bulk level. Field sites were

Special Issue: Iron Redox Chemistry and Its Environmental Impact

Received: January 12, 2019

Revised: April 26, 2019

Accepted: May 16, 2019

Published: May 16, 2019

selected where Fe(II) and oxygen coexist out of equilibrium (at least initially) but the abiotic Fe(II) oxidation rate was expected to vary by orders of magnitude.

Many years of research have resulted in comprehensive descriptions of rates and mechanisms of abiotic Fe(II) oxidation, which guided the search for locations with rapid abiotic rates. Stumm and Lee¹⁷ were the first to quantify rates of abiotic iron oxidation, and their results demonstrated that oxidation rates in dilute solution are extremely sensitive to pH between values of approximately 4 and 8, with a one pH unit increase leading to more than 1 order of magnitude increase in the observed Fe(II) oxidation rate. In this pH range, Stumm and Lee¹⁷ gave this iron oxidation rate law:

$$-\frac{d[\text{Fe}^{2+}]}{dt} = k[\text{Fe}^{2+}][\text{OH}^-]^2[\text{O}_2] \quad (1)$$

where brackets indicate concentration and k ($\text{l}^2 \text{mol}^{-2} \text{atm}^{-1} \text{min}^{-1}$) represents the rate constant. At ambient conditions, rates at pH values less than ~ 4 and greater than 8 were shown to be independent of pH.^{18,19} Millero¹⁹ made it clear that this type of dependence of the rates of oxidation on pH is driven by Fe(II) speciation. Fe^{2+} is the dominant species at low pH values. Hydrolysis becomes significant at $\text{pH} > 4$, leading to the formation of FeOH^+ , $\text{Fe}(\text{OH})_2(\text{aq})$, and $\text{Fe}(\text{OH})_3^-$ species. The relative abundances of these hydroxide complexes increase and become dominant as pH increases. The oxidation rates of ferrous hydroxide species become orders of magnitude faster with each subsequent association and are all orders of magnitude faster than the oxidation of Fe^{2+} .^{19,20}

Laboratory experiments in dilute solution helped establish rates and mechanisms of Fe(II) oxidation but are not always sufficient to explain observations in nature. Natural systems can contain thousands of solutes and contain minerals, organic matter, and microbes. Inorganic solutes can slow or hasten oxidation rates by changing the speciation of Fe(II), with each species having a unique oxidation rate constant.²¹ Organic solutes can both enhance or slow Fe(II) oxidation,²² with many common organic acid ligands stabilizing Fe(II) in solution. Mineral surfaces can also catalyze oxidation heterogeneously. Ferric mineral products of microbial and abiotic oxidation have both been shown to catalyze Fe(II) oxidation.^{9,10,23} The mechanism is thought to involve sorption of Fe(II) to surfaces of ferric mineral products, which lowers the activation energy for Fe(II) oxidation. Geochemical analysis of water and minerals, and subsequent speciation calculations, can indicate which species or minerals are driving abiotic rates in a system. The inherent complexity of factors contributing to abiotic Fe(II) oxidation rates inhibits prediction of those rates and often requires that rates in natural systems be measured directly.

The sites sampled in this study all contain significant concentrations of dissolved inorganic carbon (DIC), and in most systems bicarbonate or carbonate is the most abundant anion. Millero et al.²⁴ used equilibrium constants for the formation of ferrous bicarbonate and carbonate ((bi)-carbonate) species from Bruno et al.²⁵ to calculate the speciation of ferrous iron in natural waters and determined that complexes include FeHCO_3^+ , $\text{FeCO}_3(\text{aq})$, $\text{Fe}(\text{CO}_3)_2^{-2}$, and $\text{Fe}(\text{OH})(\text{CO}_3)^-$. Experiments by King²⁶ quantified the oxidation rates of these individual aqueous (bi)carbonate complexes. King's data are widely used to estimate ferrous iron oxidation rates in (bi)carbonate-rich natural systems. The

apparent overall rate can be expressed as a sum of the oxidation rates of the individual aqueous species:²⁶

$$-\frac{d[\text{Fe}^{2+}]}{dt} = k_{\text{app}}[\text{Fe}^{2+}][\text{O}_2] \quad (2)$$

$$k_{\text{app}} = 4(k_1\alpha_{\text{Fe}^{2+}} + k_2\alpha_{\text{FeOH}^+} + k_3\alpha_{\text{Fe}(\text{OH})_2(\text{aq})} + k_4\alpha_{\text{Fe}(\text{OH})_3^-} + k_5\alpha_{\text{Fe}(\text{CO}_3)_2^{-2}} + \dots k_n\alpha_n + \dots)$$

where α stands for the fraction of the total Fe(II) in solution accounted for by each aqueous species and k represents the second-order rate constant for oxidation by oxygen of the specified aqueous species. The individual rates are multiplied by 4 to account for the stoichiometry of 4 mol of Fe(II)/(mol of O_2). Speciation calculations can be performed to determine how much of the rapidly oxidizing ferrous (bi)carbonate species are present. It should be noted that there is still some debate on the exact speciation of ferrous iron in bicarbonate media, given the limited experimental data available^{27,28} (but see below).

When the concentration of O_2 is constant, the rate expression simplifies to the pseudo-first-order expression:

$$-\frac{d[\text{Fe}^{2+}]}{dt} = k_{\text{ox}}[\text{Fe}^{2+}] \quad (3)$$

where k_{ox} (min^{-1}) represents the pseudo-first-order rate constant. This simplified rate expression is commonly reported from field experiments because it encompasses the sum of all processes and allows rates to be directly compared among systems. It also permits the sum of the abiotic processes to be distinguished from biotic rates. Values measured in this study are calculated from eq 3 and reported as k_{ox} .

Taken together, the geochemical data, sediment compositions, rate measurements, Fe speciation calculations, and community compositions permit an integrated description of iron transformation in cold natural systems. These data can provide a foundation from which to discuss the habitability of Fe(II) oxidation in various contexts, including active systems, ancient oceans, and extraterrestrial environments.

2. METHODS

2.1. Site Descriptions. Samples were taken in September 2015 from springs and lakes in four areas of Graubünden canton in the Swiss Alps: (1) Rablönch, (2) Val Sinestra, (3) Alvaneu Bad, and (4) Jöri lakes (see map, Figure S2). Locations were chosen for samples and experiments based on apparent iron redox processes, including abundant reduced iron, significant iron minerals, or staining, or preliminary data from a 2012 scouting trip (Table S7). Rablönch (area 1) is an iron-rich spring 1 km east of the town of Scuol. The outflow forms a carbonate terrace stained with iron oxides (see map, Figure S3). Samples and experiments were performed at several locations in the outflow channel, where significant changes in pH, Fe^{2+} , and O_2 (aq) were observed (Figure S4). Val Sinestra (area 2) is located approximately 6 km to the northeast of Rablönch and contains four sources rich in iron, arsenic, and inorganic carbon. The springs were used historically as a folk remedy and are located in a dilapidated bathhouse (see map, Figure S5). Samples and experiments were performed at two springs around Alvaneu Bad (area 3), which contains numerous iron- and sulfide-rich springs and is located 3 km east of the town of Filisur. Field data for these

Table 1. Field Measurements from Spring Sources and Outflows^a

area ^b	sample ID ^c	description	pH	cond, μS/cm	T, °C	O ₂ (aq), μm ^d	Fe ²⁺ , μm ^d	lat. UTM 32T	long. UTM	elevation, masl ^e	
1	150907E ^f	layered iron mat	6.32	1674	11.1	162	93.2	600889	5184393	1190	
	150908J ^f	Fe-ox stained travertine terrace	7.67	1657	12.7	318	28.3	600893	5184375	1183	
	150907G ^f	travertine terrace without Fe-ox stain	7.91	1401	10.7	327	4.2	600896	5184374	1183	
	150907MR1	Rablönch ^g spring source in concrete housing	5.99	1795	11.1	3.4	ND	600887	5184425	1194	
	150907MR2	Rablönch water collection pipe	6.09	1790	11.2	7	ND	600889	5184414	1192	
	150907MR3	outflow below 150907MR2	6.36	1755	11.3	94	ND	600889	5184414	1191	
	2	150906B ^f	Conradin spring	6.62	5140	7.9	103	125.3	601934	5189515	1477
150906C ^f		spring below trap door	6.11	2886	8.6	1.4	166	601935	5189513	1477	
150906D		Ulrichs ^g pool	7.00	6510	8.7	159	1.4	601928	5189517	1477	
150906MR2		Ulrichs ^g source	6.38	6780	8.9	8	141	601928	5189517	1477	
150906MR1		shallow pool in back of bathhouse	6.77	2175	9.1	206	0.9	601931	5189520	1477	
150908H		pipe outflow from 150906C	6.28	2892	8.5	105	152	601964	5189509	1470	
150908I		La Brancia Creek ^g	8.27	257.4	5.3	319	BDL	601965	5189513	1470	
3		150905A ^f	Arvadi spring ^g	7.93	1118	7.8	314	2.5	548783	5168030	929
		150911T ^f	Eisenquelle	7.34	1502	7.9	5	5	551098	5168699	961

^aField measurements of outflows channels indicated on the maps (Figures S4 and S5) are depicted in Figures S4 and S6. ^bAreas correspond to designations on Figure S2 and refer to Rablönch, Val Sinestra (see section S2), and Alvanu bad (section S2). ^cSample IDs in bold have complete geochemical suites, nonbolded IDs only have field data. ^dDetection limits are 0.8 μm for Fe^{2+} and 0.15 μm for dissolved oxygen. ND, not determined; BDL, below detection limit. ^emasl = meters above sea level. ^fIron oxidation experiment location. ^gOfficial name.

Table 2. Jöri Lake Field Measurements

sample ID	lake no.	pH	cond, $\mu\text{S}/\text{cm}$	T , °C	$\text{O}_2(\text{aq})$, μm	Fe^{2+} , μm	lat. UTM 32T	long. UTM	elevation, masl
150909K	XIII at surface	6.64	7.1	9.7	293	0.4	573286	5180755	2639
150909N ^a	XIII 10 m ^b	5.76	14	7	218	15.6	573337	5180800	2629
150909L	XIII outflow	7.08	6.8	9.9	293	0.2	573337	5180800	2639
150909M ^a	XXI	9.03	25.6	8.1	336	BDL	573334	5180422	2668
150910O ^a	II	6.98	30.7	7.2	320	BDL	574139	5181021	2491
150910Q	XIX	7.36	28.8	6.6	321	BDL	573423	5180059	2720
150910R	XVIII	7.18	29.1	6.5	321	0.4	573512	5180001	2731
150910S	XXIII	8.94	33.5	3.8	343	BDL	573568	5179889	2737
150910P	snow sample	6.69	4.6	8.5	251	ND	573268	5180598	2648

^aIron oxidation experiment location. ^bSample collected from 10 m depth.

springs (areas 1–3) are shown in Table 1. The Jöri lakes (area 4) are high-elevation lake catchments with dilute water (see map, Figure S7). Ferrous iron was present in lake sediments and the water column of some lakes, while ferric mineral staining is apparent in most lakes. GPS coordinates for each sample location are shown in Tables 1 and 2, together with field geochemical data. An extended description of the springs and lakes is found in section S2 of the Supporting Information and includes maps, solute profiles of spring outflow channels, and results from a preliminary sampling trip.

2.2. Geochemistry. Complete geochemical suites were collected to provide compositional context for each rate experiment and include field measurements, water chemistry, and sediment characterization. Field measurements include meter measurements of pH, temperature, conductivity, dissolved oxygen, and ferrous iron. Water samples were analyzed for major ions, dissolved organic carbon (DOC), dissolved inorganic carbon (DIC), trace elements, $\delta^{18}\text{O}_{\text{water}}$, $\delta^2\text{H}_{\text{water}}$, and small organic anions. Sediments were analyzed for mineral composition by X-ray diffraction (XRD) and sediment iron.

2.2.1. Water Sampling and Analysis. Temperature, pH, conductivity, and dissolved oxygen were measured with portable meters in the field. The pH meters (WTW 3110) and probes (WTW Sentix 41) were calibrated daily at ambient

temperatures. Conductivity was measured using a YSI 30 m. Dissolved oxygen was measured using a fluorescence method with a detection limit of 15 parts per billion (ppb) and a resolution of ± 4 ppb (Fibox 4 m and optical probe, PreSens Inc., Germany). Ferrous iron was determined with a modified 1,10-phenanthroline method (see below).

Water was collected into a 1 L Nalgene bottle for both experiments and geochemistry using either a 140 mL syringe or 1 L high-density polyethylene (HDPE) bottle. All collection tools were acid-washed prior to the trip and rinsed with source water between samples. Samples were filtered through 1.2 μm and 0.8/0.2 μm poly(ether sulfone) (PES) syringe filters (Acrodisc 32 mm PF syringe filter with Supor filters), in series, that were rinsed with 20 mL of water before sample collection. Aliquots were collected in the order listed here to minimize contamination. Samples for stable isotopes of oxygen and hydrogen were collected without headspace in 40 mL square glass vials with polymer-lined caps for gastight storage (Qorpak). Samples for cations and anions were collected in separate 30 mL HDPE bottles that had been rinsed with 10% HCl (Omnitrac grade, Sigma-Aldrich), and then triple rinsed with 18.2 M Ω -cm ultrapure water. The cation sample bottle was spiked with 1 mL of 6 N methanesulfonic acid. Both bottles were allowed 5–10 mL of headspace for expansion during sample freezing begun on the evening of collection.

DIC samples were collected in 40 mL brown borosilicate vials with butyl rubber stoppers. DOC samples were collected in the same type of vials, with Teflon-lined silicone stoppers and spiked with 1 mL of concentrated H_3PO_4 . The DIC and DOC samples were filled completely to eliminate head space and quickly sealed to minimize degassing. Trace elements were collected in HCl-rinsed 60 mL HDPE bottles containing 800 μL of trace-metal-free concentrated nitric acid. Organic acid samples were collected last in muffled brown borosilicate glass vials with deionized-water-rinsed Teflon caps. Field blanks were collected with the same sampling equipment and methods with 18.2 M Ω -cm deionized water brought to the field in 1 L HDPE bottles that were cleaned in the laboratory with HCl and water rinses.

For water analyses, stable water isotopes ($\delta^{18}\text{O}$, $\delta^2\text{H}$) were determined with off-axis integrated cavity output spectroscopy (Los Gatos Research) using methods previously outlined.²⁹ Values are reported relative to Vienna Standard Mean Ocean Water (VSMOW). Major cations (Na^+ , K^+ , NH_4^+ , Ca^{2+} , and Mg^{2+}) and anions (SO_4^{2-} , Cl^- , Br^- , F^- , NO_3^- , and NO_2^-), as well as organic anions (formate, acetate, and lactate) were measured using ion chromatography (IC). Cations and anions were determined on two Dionex DX-600 IC systems using suppressed conductivity detectors. The anion system used S11-HC/AG11-HC columns, a potassium hydroxide eluent generator, and a carbonate removal device. The cation system used CS-16 and CG-16 columns, and cations were eluted isocratically with 19 mM methanesulfonic acid (MSA). Organic anions were determined on a Dionex ICS-1500 system using an ICE-AS6 ion exclusion column and 0.4 mM heptafluorobutyric acid eluent. DIC and DOC concentrations and carbon isotopic compositions were determined on a total organic carbon (TOC) analyzer, followed by isotope ratio mass spectrometry (IRMS). Isotopic values of C are reported relative to Pee Dee Belemnite (PDB) standard. Further details concerning these methods are given in the refs 29–32.

To determine Fe(II), a new 1,10-phenanthroline based photometric method was developed that permits data to be measured up to 3 months after sample collection. Samples for ferrous iron (3.0 mL) were taken directly with a syringe and immediately filtered through a 0.2 μm PES filter into a 5 mL plastic vial containing 100 μL of 10 g/L 1,10-phenanthroline monohydrate in 0.1 M glycine/HCl buffer adjusted to pH 2.3. Laboratory experiments with standard solutions showed this method preserved ferrous iron for later measurement for more than 3 months. The method did not reduce ferric ions or oxidize ferrous iron. Samples with $\text{Fe}^{3+}/\text{Fe}^{2+}$ ratios of up to 100:1, which can cause inaccurate results with some photometric methods, were determined accurately. This method was tested and used in several harsh natural systems, including acidic hot springs and acid mine drainage. The detection limit is 0.01 mg of Fe(II)/L, with a total uncertainty of ± 0.01 mg/L for a field measurement.

2.2.2. Sediment Sampling and Analysis. Sediment samples were collected with a variety of cleaned Teflon spoons, scoops, and tweezers that were sterilized with ethanol between locations. Each sample was collected into a new 100 mL sterile sample cup. Aliquots for DNA were transferred into 1.8 mL cryovials and immediately frozen on dry ice. Samples for XRD, reducible iron, and sediment C were placed in 5 mL cryovials and also frozen on dry ice in the field. Larger pieces of sediment were placed into sterile whirlpak bags and frozen later in the day.

Carbon content and isotopic composition of sediments were determined by elemental analysis–isotope ratio mass spectrometry (EA-IRMS) on a Costech elemental analyzer and a Thermo Delta plus Advantage IRMS apparatus.³⁰ Samples were prepared by drying sediments at 50 °C overnight, grinding to a fine powder, and drying again overnight. Samples for total carbon analysis were prepared by weighing ~ 100 mg of sediments in tin capsules to the nearest microgram. Organic carbon analyses were prepared the same way, except they were repeatedly acidified with high-purity 3 M HCl (OmniTrace) in silver capsules.

Mineral composition of sediments was analyzed by powder X-ray diffraction (XRD). Samples were dried at 50 °C overnight before being powdered using an agate mortar and pestle. Approximately 200 mg were mixed with isopropanol and applied to quartz zero-background slides. Mineral identification was performed by XRD using Cu $K\alpha$ radiation from 4° to 90° 2 θ , with a step size of 0.016° and rate of 0.850 s/step with a Siemens D5000. The XRD system was run at 40 kV and 40 mA. Resulting diffractograms were analyzed using the JADE XRD software.

Sediments were characterized for their poorly crystalline ferric mineral content by the method outlined by Lovley and Phillips,³³ which allows for rapid quantification of minerals that are available to microbial iron oxidizers. Ferrous iron in sediments was measured by adding approximately 100 mg of freshly weighed sediment to 5 mL of 0.5 M HCl (OmniTrace). Samples were vortexed and allowed to sit for 1 h. Fe(II) was measured using the ferrozine method³⁴ in 4-(2-hydroxyethyl)-1-piperazineethanesulfonic acid (HEPES) buffer adjusted to pH 5.5. The total readily reducible iron content of the sediments, including amorphous ferric minerals and Fe^{3+} , were determined by the same method, except a solution of 0.25 M hydroxylamine and 0.25 M HCl was used to reductively dissolve minerals. Ferric iron was then determined by subtracting the measured Fe(II) from the total iron.

2.3. Iron(II) Oxidation Rate Experiments. Experiments were designed to measure the rates of biological and abiological Fe(II) oxidation reactions in situ. Microcosm experiments were performed using sediment and sample water at the field site. Two protocols were used, with the choice being determined by the anticipated duration of the experiment. The following standard protocol was used in systems where ferrous iron was not anticipated to be depleted for at least 20 min. Typically, 10 g of sediment and 40 mL of spring water were combined in a 60 mL serum bottle. Each assay included an added-Fe(II) treatment, an unamended treatment, and a killed control. Treatments were assayed in triplicate. The added-Fe(II) treatment included addition of 50 μM Fe(II) (as $\text{FeSO}_4 \cdot 7 \text{H}_2\text{O}$) to samples from springs with native concentrations less than 25 μM , while 150 μM Fe(II) was added to samples from all other systems. This range in Fe(II) allowed an assessment of maximum metabolic capacity of each system and better resolution of rate constants. Killed controls were fixed with 6 mM sodium azide that had its pH matched to the spring. All chemical fixatives have some uncertainty surrounding their effectiveness and potential for secondary reactions, but 6 mM sodium azide has previously been shown to be effective at inhibiting FeOB,⁹ does not interfere with Fe(II) method, and has been shown to not oxidize or reduce iron at the conditions of the sample locations. These killed controls had the same amount of additional Fe(II) as the added-Fe(II) treatments. A summary of treatment parameters

is given in Table 3. Measurements of ferrous iron concentration were assayed by the sampling method outlined

Table 3. Microcosm Rate Experiment Parameters

	treatment	iron source, $\mu\text{M Fe(II)}^a$	sterilization
standard protocol	added Fe(II)	50–150	<i>b</i>
	unamended	<i>b</i>	<i>b</i>
	killed	50–150	6 mM azide
rapid oxidation protocol	ROP-added Fe(II)	56	<i>b</i>
	filtered	56	0.2 μM filtration

^aFe(II) from $\text{FeSO}_4 \cdot 7\text{H}_2\text{O}$. ^bNot applied to this treatment.

above at a time interval appropriate for the anticipated abiotic rate. The interval was around 30 min for springs with $\text{pH} < 7$ and 10 min for springs with $\text{pH} 7\text{--}7.5$.

An alternate protocol was used in systems where ferrous iron was expected to be fully depleted in the experiments in less than 20 min (*rapid oxidation protocol*). Modifying the protocol permitted more accurate rate measurements at these kinetic extremes. The duration of an experiment during which microcosm water is equilibrating with the atmosphere, coupled with the typically low concentration of Fe(II) in these locations, can create variations in reaction progress and pH before data collection can begin. These difficulties can lead to large uncertainties that impede distinguishing rates among treatments. To compensate, all treatments included added ferrous iron. Replicates were performed sequentially to minimize equilibration time, with water drawn directly from the sample location with a syringe and immediately added to a serum vial. Reagents were appended immediately. Duration was measured from the moment the Fe(II) reagent was added. Treatments included a rapid oxidation protocol-added-Fe(II) (ROP-added-Fe(II)) microcosm and a filtered control, each with 3 replicates. The ROP-added-Fe(II) treatment is the same as the added-Fe(II) standard procedure described above and provides rates inclusive of all biotic and abiotic processes. The filtered treatment consisted of 0.2 μM filtered water from the natural system to provide abiotic oxidation rates. Both treatments had $\sim 56 \mu\text{M}$ added Fe(II) (see Table 3). Results of several iterations of various sample protocols revealed that filter sterilization is the most representative of in situ abiotic rates in situations where abiotic oxidation is extremely rapid. The primary objective of this treatment is to minimize oxidation of components in the sample fluid and maintain the system pH by minimizing degassing, precipitation, and dissolution of atmospheric O_2 . A limitation of this treatment is that any mineral catalysis is unmeasured, although these changes to the rate are expected to be minor relative to the rate of reaction in solution. Test experiments show that addition of sodium azide required several minutes of equilibration before measurements of Fe(II) and pH are reliable, even when the pH of the azide solution is matched to the pH of the system.

2.4. Community Composition. DNA extraction from sediments for community identification was performed in Prof. Eric Boyd's laboratory at Montana State University, using methods analogous to those of Colman et al.³⁵ Briefly, approximately 250 mg of thawed sediment or mat sample was used with a DNA extraction kit (MP Biomedical FastDNA spin kit for soils). DNA was quantified with the Qubit DNA assay kit and a Qubit 2.0 fluorimeter (Life Technologies). PCR was

performed using universal 16s rRNA primers 515F (GTGCCAGCMGCCGCGGTAA) and 806R (GGAC-TACHVGGGTWTCTAAT). An $\sim 1 \text{ ng}$ amount of purified genomic DNA was subjected to PCR in triplicate using an initial denaturation at 94°C (4 min), followed by 35 cycles of denaturation at 94°C (1 min), annealing at 55°C , primer extension at 65°C (1.5 min), and a final extension step at 65°C (20 min). The PCR mixture contained 2 mM MgCl_2 , 200 μM deoxynucleotide triphosphate, 0.5 μM each forward and reverse primer, 0.4 mg/mL bovine serum albumin, and 0.25 units of Taq DNA polymerase in PCR buffer (all reagents, Invitrogen) for a total volume of 50 μL . A 4 μL aliquot of each PCR product was run on a 2% agarose gel to ensure amplification. Triplicate PCR products were then pooled and purified using the Wizard PCR cleanup system (Promega) per the instructions, yielding a final volume of 50 μL . DNA was quantified again using the Qubit system. PCR products were sent to the MrDNA laboratory (Molecular Research LP, Shallowater, TX, USA) for sequencing using the Illumina MiSeq system with $>30,000$ reads per assay. Postprocessing was performed with Mothur³⁶ using methods previously described.^{35,37} Briefly, the paired reads were merged and trimmed to a maximum length of 250 bases, with chimeras removed. Operational taxonomic units (OTUs) were assigned at a sequence similarity of $\geq 97\%$ using the nearest neighbor method and classified using the latest Silva database.^{38,39} Chloroplast and mitochondrial 16s reads were removed. Figures used in this work rely on these Silva database results. For better taxonomic resolution, OTU sequences at $\geq 1\%$ abundance for each sample location were manually searched with the NCBI 16s rRNA sequence library using the BLASTn tool. A complete listing of those results can be found in the Supporting Information.

2.5. Speciation Calculations. Speciation calculations were performed with compositional data from each system using the EQ3 software package.⁴⁰ Thermodynamic data used for these speciation calculations were taken from Helgeson et al.,⁴¹ Shock et al.,^{42,43} Shock and McKinnon,⁴⁴ Sverjensky et al.,⁴⁵ and Shock,⁴⁶ together with estimates obtained in this work as described in section S1 of the Supporting Information. Briefly, thermodynamic properties of FeHCO_3^+ , $\text{FeCO}_3(\text{aq})$, $\text{Fe}(\text{CO}_3)_2^{-2}$, NaCO_3^- , $\text{NaHCO}_3(\text{aq})$, KCO_3^- , KHCO_3 , NH_4CO_3^- , and other relevant carbonate and bicarbonate aqueous species were estimated using the methods outlined in section S1.^{45,47–49} Equilibrium constants for these species at 25°C and 1 bar reference conditions were obtained from the literature (see section S1 of the Supporting Information for references). The thermodynamic properties were used to generate equilibrium constants at appropriate temperatures calculated with the revised Helgeson–Kirkham–Flowers equation of state⁵⁰ using the CHNOSZ software package.⁵¹ These equilibrium constants were used to add the metal (bi)carbonate species to a thermodynamic database consistent with the references above and an extended Debye–Hückel equation for activity coefficients.⁵² See section S1 of the Supporting Information for details.

3. RESULTS AND DISCUSSION

3.1. Rate Experiments. Experiments to determine the rate of biological and abiotic iron oxidation were performed at 10 locations. The systems chosen for these experiments vary dramatically in geochemical composition, but all showed evidence that they host iron oxidation. A primary objective of

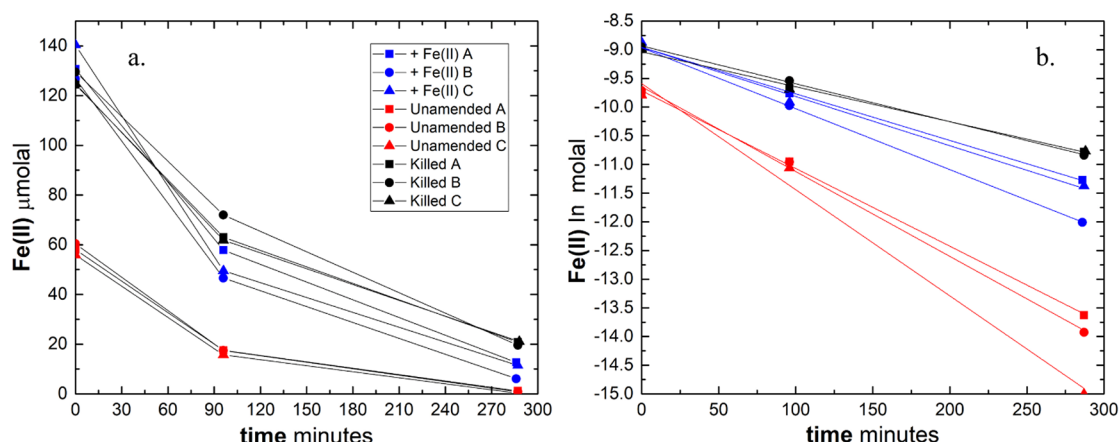


Figure 1. Iron oxidation experimental results (150907F) for a Rablönch iron mat, using the standard rate experiment protocol. Analogous plots for other experiments can be found in [section S3](#) of the Supporting Information. Blue, red, and black points represent added Fe(II), unamended, and killed treatments, respectively. The three shapes correspond to one of three replicates for each treatment. Panel a shows data as collected during field experiments. The added-Fe(II) (blue) and killed (black) points both have added ferrous iron, which is why the initial concentration is higher than the unamended (red) points. Panel b shows the same data plotted on a natural logarithmic scale, revealing the first-order kinetics of the reaction. Lines reflect linear fits that are indicative of the rate constant.

the experiments was to determine the conditions that favor biological oxidation, as well as the conditions that exclude biology. Biological oxidation was detected at six locations, while abiotic rates were determined at all 10 experiment locations. Abiotic rates ranged from inconsequential, to oxidation too fast for biology to compete. Results show pH and DIC as major determinants of biological iron oxidation activity.

The standard protocol allowed measurement of three rates: the overall in situ rate (unamended treatment), the abiotic rate (killed control), and a Fe(II) substrate enhanced rate (added Fe(II) treatment), each determined in triplicate (see parameters in [Table 3](#)). A representative example of data collected during a field experiment using the standard protocol at field site 150907F, an iron mat at Rablönch, is shown in [Figure 1](#) (data in [Table S5](#)). Changing concentrations of Fe(II) over the duration of the experiments are shown in [Figure 1a](#). The unamended measurements (red points) have an initial Fe(II) concentration equal to that found naturally in the springs, which approaches the detection limit after ~ 275 min. This near complete Fe(II) depletion means the measured rate is a minimum value, as the time elapsed when the experiments become fully depleted can only be constrained to duration between measurements. The results from these unamended treatments are inclusive of both biotic and abiotic oxidation. Added Fe(II) treatments (blue points) featured $\sim 50 \mu\text{M}$ Fe(II) added to assess the maximum capacity of the system to oxidize iron. In this case, the replicate initial concentrations are $130 \mu\text{M}$, which decrease to $20 \mu\text{M}$ after ~ 275 min. The abiotic rate was determined from the killed controls (black points). These replicates contain the same initial concentration of Fe(II) as the added-Fe(II) treatments, except that 6 mM azide was added to inhibit growth. The initial concentrations are also close to $130 \mu\text{M}$, but are depleted to only $30 \mu\text{M}$ after ~ 275 min. The differences in rates between the black and blue points are attributable to FeOB in the sediment.

The same experimental data are plotted as the natural log of the Fe(II) concentration in [Figure 1b](#). The linearity of the plots in [Figure 1b](#) reveal pseudo-first-order kinetics for these field experiments; the slopes of the lines yield rate constants, k_{ox} for the oxidation reactions. Rate constants are the most

directly comparable measurements among replicates and between systems, as they are independent of the initial concentration of Fe(II). The greater rate constants exhibited by unamended and added-Fe(II) treatments indicate rates that are enhanced by iron oxidizers compared with the killed controls. Rate measurements from all standard protocol experiments, including rate constants, rates, and half-lives, can be found in the upper part of [Table 4](#), and plots analogous to [Figure 1](#), together with the experimental data for all standard protocol experiments, are collected in the Supporting Information ([Tables S2–S7](#) and [Figures S8–S12](#)).

In situations where ferrous iron is depleted in less than 20 min, the standard protocol is not sufficient to resolve differences in rates between treatments. In such systems the rapid oxidation protocol was implemented to attempt to distinguish biotic rates from the rapid abiotic process and to provide greater resolution. An example of data from field experiments using the rapid oxidation protocol at site 150907G, an outflow of Rablönch on unstained travertine, is shown in [Figure 2](#) (data in [Table S15](#)). The plots are analogous to those in [Figure 1](#), but note the much shorter duration of experiments. The ROP-added-Fe(II) treatments (blue points) include sediment, water, and an additional $\sim 55 \mu\text{M}$ of Fe(II). The filtered treatments (black points) have only $0.2 \mu\text{M}$ of filtered spring water and added $\sim 50 \mu\text{M}$ of Fe(II). In this example, biological iron oxidation was not detected in the experiments that include sediments, leading to the conclusion that the observed rate is dominated by abiotic processes. The filtered, abiotic rate slightly exceeded that of the FOP-added-Fe(II) treatment, suggesting that processes in addition to oxidation may be happening. Possibilities include desorption of Fe(II) from the sediments or increased chelation from organic compounds in the sediments, either of which would make the concentration of Fe(II) appear to decrease using the 1,10-phenanthroline test. If the change in concentration is driven by extremely rapid chemical oxidation, any increase in the rate owing to heterogeneous oxidation by ferric minerals is negligible. Rate data from all rapid oxidation protocol experiments can be found in the lower section of [Table 4](#). Reported data include rate constants, half-lives, and initial rates for each replicate. The abiotic component of the rate is

Table 4. Results of in Situ Rate Experiments^a

sample ID	replicate	added Fe(II)				unamended				killed			
		log(<i>k_{av}</i> /min ⁻¹)	half-life, min	$\frac{d[Fe^{2+}]}{dt}$, μmol min ⁻¹	av rate, μmol min ⁻¹	log(<i>k_{av}</i> /min ⁻¹)	half-life, min	$\frac{d[Fe^{2+}]}{dt}$, μmol min ⁻¹	av rate, μmol min ⁻¹	log(<i>k_{av}</i> /min ⁻¹)	half-life, min	$\frac{d[Fe^{2+}]}{dt}$, μmol min ⁻¹	av rate, μmol min ⁻¹
150907F	A	-1.972	65	0.45	0.42	-1.733	37	0.34	0.29	-2.215	114	0.243	0.25
	B	-1.974	65	0.43		-1.868	51	0.26		-2.210	112	0.256	
	C	-2.067	81	0.39		-1.830	47	0.27		-2.180	105	0.264	
150906B	A	-1.815	45	0.38	0.33	-1.827	47	0.08	0.08	-2.187	107	0.093	0.12
	B	-1.915	57	0.32		-1.790	43	0.08		-2.143	96	0.111	
	C	-1.920	58	0.28		-1.775	41	0.07		-2.102	88	0.154	
150906C	A	-2.790	428	0.16	0.14	-3.137	950	0.04	0.04	-3.620	2888	0.023	0.03
	B	-2.921	578	0.12		-3.244	1216	0.03		-3.569	2567	0.026	
	C	-2.863	506	0.15		-3.131	937	0.04		-3.456	1980	0.032	
150911T	A	-1.468	16	0.64	0.43	<i>b</i>			<i>b</i>	-1.971	65	0.137	0.28
	B	-1.490	21	0.33		<i>b</i>				-1.889	54	0.275	
	C	-1.594	27	0.32		<i>b</i>				-1.717	36	0.424	
150909K	A	-2.491	215	0.06	0.05	-2.886	533	0.003	0.01	-3.886	5332	0.002	0.01
	B	-2.678	330	0.04		-2.754	394	0.010		-3.638	3014	0.006	
	C	-2.575	261	0.05		-2.387	169	0.009		-3.398	1733	0.007	
150910O	A	-1.971	65	0.10	0.08	-2.480	209	0.007	0.00	-3.237	1195	0.009	0.03
	B	-2.018	72	0.07		-2.078	83	0.004		-2.597	274	0.044	
	C	ND	ND	ND		-2.248	123	0.003		-2.509	224	0.051	
Rapid Oxidation Protocol													
ROP-Added Fe(II)													
150907G	A	0.033	0.6	12.9	15.88					0.150	0.49	7.324	8.62
	B	-0.045	0.8	10.2						0.135	0.51	9.160	
	C	0.108	0.5	24.5						0.124	0.52	9.379	
150908J	A	-0.151	1.0	15.5	8.90					-0.102	0.88	19.240	18.85
	B	-0.233	1.2	6.2						-0.119	0.91	17.413	
	C	-0.201	1.1	5.0						-0.151	0.98	19.885	
150909M	A	0.59 ^c	0.18 ^c	N/A						0.59 ^c	0.18 ^c	N/A	N/A
	B	0.59 ^c	0.18 ^c	N/A						0.59 ^c	0.18 ^c	N/A	
	C	0.59 ^c	0.18 ^c	N/A						0.59 ^c	0.18 ^c	N/A	
150905A	A	-0.096	0.87	17.5	25.3					0.231	0.407	36.6	24.5
	B	0.031	0.64	23.1						-0.083	0.839	16.4	
	C	0.262	0.38	35.4						0.259	0.382	20.5	

^aResults calculated using eq 3. N/A indicates not applicable as in situ concentration of Fe(II) was below detection limit. ^bRate not reported. Fe²⁺ in the replicate was below detection by the time the second measurement was made. ^cMinimum rate—replicate dropped below the detection limit before the experiment ended.

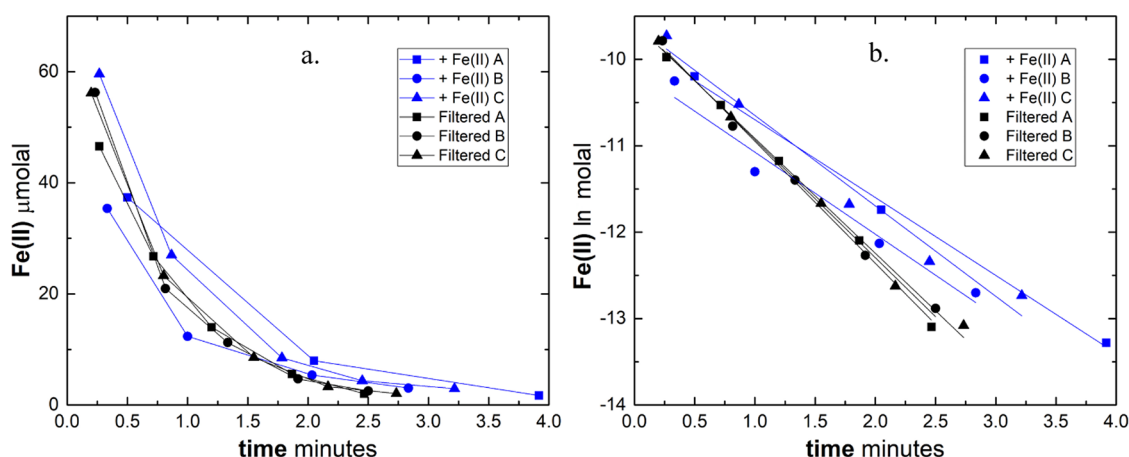


Figure 2. Fe(II) oxidation experimental results using the rapid oxidation protocol at site 150907G, an outflow of Rablönch on an unstained travertine terrace. Analogous plots for other experiments can be found in the [Supporting Information](#). Blue points represent the ROP-added-Fe(II) replicates, while black points indicate the filtered (abiotic) treatments. Panel a shows data as collected during field experiments. Both data sets have added ferrous iron (see text). Note the short duration of each experiment. The added-Fe(II) and filtered treatment rates are nearly indistinguishable, suggesting biological iron oxidation is not present. Panel b shows the same data but plotted on a natural logarithmic scale, revealing the first-order kinetics of the reaction. Lines reflect linear fits that are indicative of the rate constant.

included in the ROP-added-Fe(II) and unamended treatments, so these values are the sum of abiotic and biotic processes. Minimum rates are reported for Jöri Lake XXI (150909M) and Arvadi spring (150905A), because extremely rapid abiotic oxidation in these systems caused the concentration of ferrous iron to be depleted to close to the detection limit by the time the third data point was taken (typically less than 1 min). While both the ROP-added-Fe(II) and filtered treatments showed minimum rates, biological oxidation is presumed to be excluded in the bulk system by the lack of bioavailable ferrous iron.

Taken together, the rate experiments show that opportunities for biological Fe(II) oxidation are fundamentally determined by geochemistry, especially the pH. Results show that FeOB are responsible for the majority of the Fe(II) oxidation in systems with $\text{pH} < 7$, while the extremely rapid chemical oxidation in systems at and above $\text{pH} \sim 7.7$ effectively preclude FeOB. Results from all experimental locations summarized in [Figure 3](#) allow comparison of rate constants determined in the live microcosms (red dots) with the abiotic oxidation rate constants (black squares). The depicted live microcosm values are the average rate constant of 3 replicates of the unamended or added-Fe(II) treatments (only the ROP-added-Fe(II) treatment for rapid oxidation protocol experiments), whichever is larger. The average rate constants obtained in both treatments are typically similar, as anticipated from the reactant-independent rate law. The abiotic rate constant is the average of 3 replicates of the killed or sterilized treatment depending on the protocol for each type of experiment. Error bars indicate one standard deviation. The abiotic rate constants measured in these systems increase dramatically as pH increases, consistent with the known mechanisms and speciation models discussed below, and exceed the rate of iron oxidation in the live microcosms at $\text{pH} \geq 7.7$. Below this pH, the oxidation rate constants of the live microcosms fall in a relatively consistent range, suggesting that the in situ FeOB communities are operating efficiently near their maximum physiological capacity. At pH values ≥ 7.7 , the abiotic rates become so rapid that FeOB communities appear to be excluded.

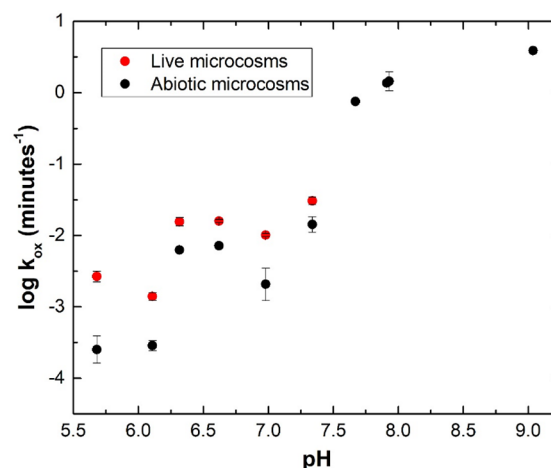


Figure 3. Rate constants from live microcosms (red) and abiotic microcosms (black) in Swiss springs and lakes. Values are the average of three replicates reported in [Table 4](#). Error bars signify ± 1 standard deviation. Live microcosms indicate either the unamended or added-Fe(II) treatment, whichever is faster; The rate constant for the unamended treatment is shown for 150906B and 150907F, while the added-Fe(II) treatment is depicted for 150906C, 150911T, 150909K, and 150910O (for sample ID see [Tables 1 and 2](#)). Live microcosm rate constants reported here are those measured in the field and do not have the abiotic contribution subtracted. The contribution of FeOB to the rate is the difference between each pair of red and black points. Abiotic microcosms indicate either killed or filtered treatment, depending on the protocol used in that experiment. Biological contribution to the oxidation of iron was not detected above pH 7.4.

It should be noted that the live microcosm rates shown in [Figure 3](#) are the sum of all biotic and abiotic processes and do not have the abiotic contributions subtracted. Therefore, the difference between the live microcosm and abiotic points represents the contribution to oxidation rate of oxidation by FeOB. These differences, represented as the percentage of Fe(II) oxidation attributable to biology, are depicted in [Figure 4](#), where it can be seen that the biological oxidation of iron could not be detected above about $\text{pH} = 7.5$. Percentages are calculated from the initial instantaneous rates (found in [Table](#)

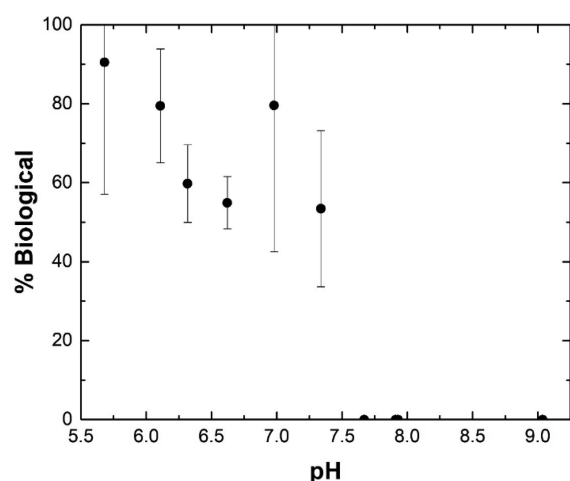


Figure 4. Percentage of oxidation attributable to biology plotted against the pH of each system. Percentages calculated from average rate constants of triplicate experiments reported in Table 4 and shown in Figure 3. Error bars represent the propagated percent standard error of three replicates of both the live and abiotic microcosms. Environments at $\text{pH} \leq 7.4$ support biological oxidation, whereas systems at higher pH values have such rapid abiotic rates that biological iron oxidation was not detected.

4), as these are most indicative of rates in the natural systems where substrate flux is constant (unlike in the microcosms). Since measured biological rates between locations typically vary by less than 1 order of magnitude, the abiotic rate dictates how much ferrous iron is bioavailable to FeOB. Considering that the solubility of Fe(II) is low at $\text{pH} > 8$, and the abiotic oxidation rate is so rapid, the maximum attainable supply of Fe(II) is unlikely to be sufficient to support communities of FeOB. These results do not necessarily completely exclude individual microbes or fleetingly small populations of FeOB at these conditions, but indicate that FeOB populations are unlikely to make large contributions to productivity in these ecosystems.

3.2. Speciation. The geochemical composition of a natural system determines the form that ferrous iron takes in solution, and ultimately dictates abiotic iron oxidation rates. As an example, increasing concentrations of bicarbonate were found to significantly increase the abiotic iron oxidation rate even while pH was kept constant.²¹ These observations led to the hypothesis that aqueous ferrous bicarbonate or carbonate complex species were responsible for the increased rates. Speciation of ferrous iron in bicarbonate media was determined by Bruno et al.,²⁵ which enabled quantification of the rate constants for individual chemical species.²⁶ Formation of these ferrous (bi)carbonate species partially explains the observed abiotic rates above. Bicarbonate and carbonate ions, which constitute the bulk of the DIC at the pH values of these samples, are also the most abundant anions in the springs and lakes in this study (Table 5), as illustrated by the plot shown in Figure 5. Conductivity is a close proxy for total dissolved ionic species, and the approximately linear distribution of points in Figure 5 suggests that conductivity is strongly influenced by the abundance of bicarbonate and carbonate ions dissolved in the water. These solutes likely reflect weathering of the abundant carbonate minerals in the region of the springs (Rablönch, Val Sinestra, and Alvaneu). Here, the carbonate, bicarbonate, and sulfate stem from ion exchange with the sediment phases of the Bünden shale

(Rablönch and Val Sinestra) and from subsurface weathering of gypsum containing dolomite (Alvaneu), respectively. At Jöri, however, the low bicarbonate and carbonate stem from chemical weathering of silicate minerals by carbonic acid. Local geology determines the second most abundant anion in these waters, which is typically either sulfate or chloride. The resulting bicarbonate-rich waters were found to strongly control the aqueous ferrous iron speciation.

In the present study, new estimates of standard state thermodynamic properties of aqueous carbonate and bicarbonate complexes permit speciation calculations at a wide variety of temperatures and pressures. The methods by which these estimates were made are detailed in section S1 of the Supporting Information. Predicted equilibrium constants for carbonate and bicarbonate complexes, together with the analytical data for major ion concentrations, pH, and DIC abundances (Table 5) allow speciation calculations. [Note that two values of DIC are reported in Table 5 for some samples. Values reported in parentheses were measured, and those calculated from considerations of charge balance were used in speciation calculations. These adjustments were made on samples for which charge imbalance was greater than 10%. Typically, samples with charge imbalances showed small amounts of precipitate in sample vials after analysis, consistent with anomalously low bicarbonate concentration.] The samples for geochemical analyses were taken at the locations where water was taken for rate experiments and as close as possible in time to the start of the corresponding experiments.

A Bjerrum diagram, calculated with thermodynamic data from section S1 in the Supporting Information, that depicts the speciation of Fe(II) at 25 °C in a solution containing millimolar DIC, is shown in Figure 6a, where it can be seen that Fe^{2+} is the most abundant species at $\text{pH} < 7$. The carbonate complexes $\text{FeCO}_3(\text{aq})$ and $\text{Fe}(\text{CO}_3)_2^{-2}$ dominate between pH 7 and 9, and $\text{pH} > 9$, respectively. The bicarbonate complex is significant around a pH of 7 but is never the most abundant species. The hydroxide species FeOH^+ and $\text{Fe}(\text{OH})_2(\text{aq})$ that dominate circumneutral ferrous speciation (and dictate rates) in dilute solution are several orders of magnitude less abundant than the inorganic carbon complexes.

Speciation calculations performed for each of the carbonate springs are summarized in Figure 6b, which shows the calculated percentages for each species (data in Table S21). Fe^{2+} , represented by black bars, is typically the most abundant species in springs with $\text{pH} < \sim 7$. The FeHCO_3^+ species is calculated to compose up to 25% of the Fe(II) in springs between pH 6 and 7 and is a minor component at higher pH values. The abundance of $\text{FeCO}_3(\text{aq})$ increases dramatically from a few percent at pH 6 to become the most abundant species at $\text{pH} > 7.5$. Owing to the DIC concentrations, $\text{Fe}(\text{CO}_3)_2^{-2}$ is a minor contributor to Fe(II) speciation at pH values greater than 7.5. Despite this feeble presence, this species can increase the rate substantially.²⁶ In addition, $\text{FeSO}_4(\text{aq})$ is a minor contributor to the speciation of Fe(II) in most samples but is the most abundant species in the spring at pH 7.3 (150911T) due to a relatively low DIC content and abundant sulfate.

The Jöri lake systems are extremely dilute (Table 5), and the bulk lake waters of most locations were below the detection limit for Fe(II). Speciation calculations were only possible on three samples (not shown), yielding results showing abundant FeOH^+ , $\text{Fe}(\text{OH})_2$, and Fe^{2+} . It can be assumed that the other

Table 5. Major Cations and Anions, Dissolved Inorganic Carbon (DIC), and Dissolved Organic Carbon (DOC)^a

sample ID	F ⁻	Cl ⁻	Br ⁻	SO ₄ ⁻²	PO ₄ ⁻³	NO ₂ ⁻	NO ₃ ⁻	Li ⁺	Na ⁺	NH ₄ ⁺	K ⁺	Mg ²⁺	Ca ²⁺	DIC ^b	δ ¹³ CDIC	DOC	δ ¹³ CDOC
150907F	8.9	907	1.55	491	BDL	BDL	1.06	31.8	2519	23.2	110	1789	11071	55.0 (35.1)	3.7	67	ND
150908J	7.9	978	0.70	478	BDL	0.07	2.64	32.4	2559	18	112	1821	10953	27.1 (16.5)	8.0	75	-15.9
150907G	16.2	980	0.989	494	BDL	0.05	2.16	32.8	2534	18.6	113	1786	9963	24.3 (15.1)	8.1	50	-21.8
150906B	27.4	27378	139.2	4064	20.20	1.15	98.75	1350	49879	356	1669	4374	14963	85.3 (66.4)	4.1	133	ND
150906C	21.4	12574	63.5	2076	BDL	BDL	2.45	445	16876	150	557	2001	7656	58.5 (49.4)	1.7	100	ND
150906D	41.9	37966	198.9	5565	BDL	BDL	57.99	1805	67070	517	2225	5118	16697	79.1 (55.5)	4.9	117	ND
150908H	19.8	12699	66.7	2103	0.07	0.04	1.96	621	23218	189	768	2722	9484	49.6 (45.7)	2.4	58	-26.5
150905A	83.4	16.3	BDL	8352	0.16	BDL	0.12	1.35	71.2	2.02	27.3	3023	7012	4.24	-3.6	25	-24.5
150911T	74.6	21.5	BDL	13784	BDL	BDL	0.33	1.07	90.1	2.21	18.4	4661	9644	2.48	-2.7	17	-22.6
150909K	7.5	2.45	BDL	10.0	BDL	BDL	0.32	0.031	11.9	1.34	2.43	4.63	25.1	0.08 (0.05)	-3	92	-20.6
150909N	7.1	2.41	BDL	9.1	BDL	BDL	0.34	0.0137	11.4	5.96	4.73	5.48	28.6	0.17	-8	117	-25.8
150909L	7.6	1.21	BDL	9.9	BDL	BDL	0.10	0.0115	9.54	1.14	2.08	3.86	21.6	0.04	2	67	-18.5
150909M	4.2	2.16	BDL	38.0	BDL	0.074	24.18	0.0274	20.5	1.21	4.7	24.4	74.3	0.18	-11	50	-20.5
150910Q	19.7	2.07	BDL	64.6	BDL	0.0304	16.72	0.0497	17.1	1.06	5.9	15.9	74.5	0.25	-5.5	42	-25.7
150910Q	4.9	2.47	BDL	36.9	BDL	0.07	27.31	0.0288	22.3	0.998	5.23	21.7	78.1	0.34	-8.0	42	-19.4
150910R	7.8	3.27	BDL	16.4	BDL	0.051	25.39	0.0504	38.5	2.31	10	36.9	148	0.40	-5.6	83	-23.2
150910S	11.7	2.14	BDL	17.9	BDL	0.04	54.12	0.036	48.6	2.01	9.19	38.1	184	0.47	-6.3	42	-23.8
150910P	0.0	0.98	BDL	0.8	BDL	BDL	15.15	0.0014	0.72	8.78	0.268	0.19	5.26	BDL	-	25	-21.8

^aUnits are in μmol/kg solution, except DIC values are reported as mmol C/kg, and DOC are reported as μmol C/kg. Isotopic compositions of DIC and DOC are reported as δ¹³C vPDB (‰). BDL, below detection limit; ND, not determined. For sample designations see Tables 1 and 2. ^bPrecipitates were observed in some DIC sample vials. For those samples, charge balance corrected values are reported while measured values are in parentheses.

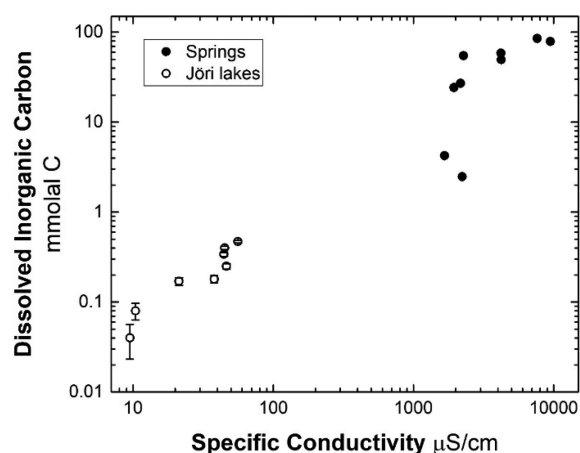


Figure 5. Dissolved inorganic carbon (DIC) in Swiss Jöri mountain lakes and springs plotted against measured conductivity. Weathering of local carbonate rocks makes bicarbonate and carbonate ions abundant in solution, and as a result DIC increases with conductivity. The origin of DIC in the springs is as follows: Rablönch and Val Sinestra, release of bicarbonate from shale deposits of the former Tethys ocean; Alvaneu springs, subsurface dissolution of midtriassic dolomite. The DIC in the Jöri lakes is up to 1000× less than in the springs. In the Jöri catchment DIC stems from the weathering of silicate gneiss rocks by carbonic acid from the atmosphere. The atmospheric carbonic acid loses a proton during the weathering process and becomes bicarbonate.

lakes' samples would be speciated in similar ways given their similar compositions that are low in DIC. Biological iron oxidation in the lake sediments is likely happening at the oxic/anoxic boundary in the sediments, as suggested by 1–2 cm bands of iron oxide at approximately 3 cm sediment depth in Jöri Lake 2. Pore water compositions reported by Steiner et al.⁵³ also suggest elevated ferrous iron in the sediments relative

to the overlying water. The sediment pore waters are likely to speciate similarly to the overlying water due to the low DIC concentration, suggesting abiotic oxidation rates would be similar to those found in laboratory experiments on dilute solutions.^{17,19}

Overall, the speciation results provide an additional layer of information for explaining the observed oxidation rates. They show that ferrous iron speciation in the springs is dominated by ferrous (bi)carbonate complexes and Fe^{2+} . As a result, the speciation results demonstrate that laboratory studies on oxidation rates for individual aqueous species can be relevant to natural ferrous iron containing systems with relatively abundant DIC. Our rate experiments do not allow us to elucidate rate constants for individual species (eq 2), but the combined results implicate speciation as contributing to the rapid abiotic rate and thereby excluding FeOB.

3.3. Sediments. Most microbes, including the majority of FeOB, are found in the sediments in these springs and lakes. Characterizing the sediments for organic carbon and iron content permits estimates of the biomass content and identity and extent of mineral product formation. Results of sediment analysis, including minerals (XRD), total and organic carbon (EA), and their isotopic compositions (IRMS) are given in Table 6.

3.3.1. Carbon in Sediments. Cold spring sediments primarily contain carbonate minerals, and calcite and dolomite are the most common phases identifiable by XRD. Ferric minerals were not identified by XRD, despite the deep red staining observed in the springs. The organic carbon content of the spring sediments is typically low, with values ranging from 0.09–0.25%. The organic C is always isotopically light, -23.4 to -29.5 . Most springs do not contain significant plant detritus, so these values are likely indicative of microbial biomass. One exception is Arvadi at 0.92% organic C, which contains abundant decaying forest debris. All of the springs

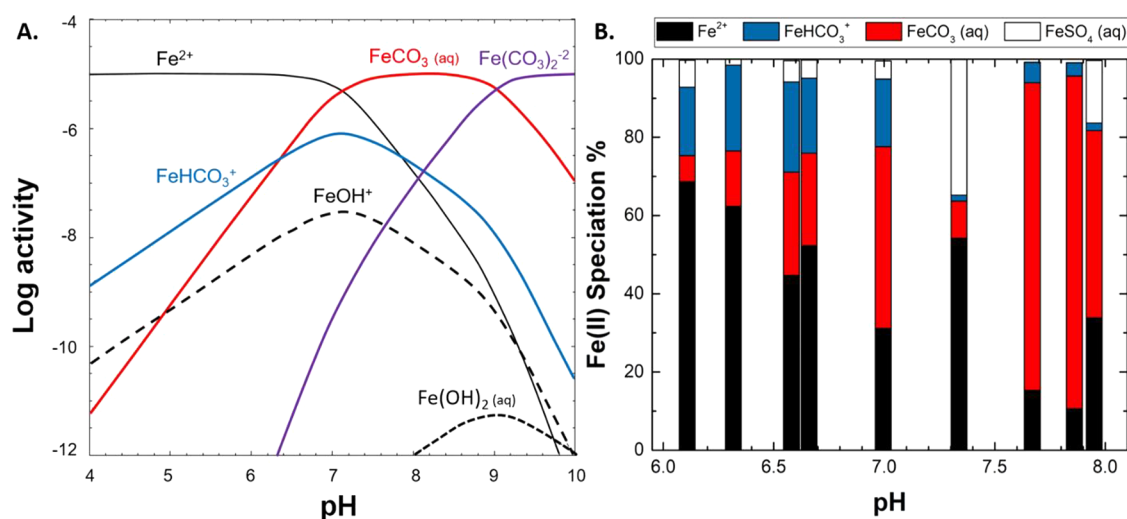


Figure 6. Calculated speciation of Fe(II) in bicarbonate media. (a) Bjerrum diagram showing the speciation of Fe(II) in aqueous solution at 25 °C, containing 10^{-5} M total Fe(II) and 10^{-5} M total CO_3^{2-} . Equilibrium constants taken from literature values reported in section S1 of the Supporting Information. This plot was calculated using the CHNOSZ software package,⁵¹ together with a modified database developed in this study (see section S1 in the Supporting Information). (b) Speciation of Fe(II) in iron springs. Pairs of springs at pH values of both 6.6 and 7.9 have been offset on the plot to allow all four speciation results to be visible. Black, blue, red, and white bars represent Fe^{2+} , FeHCO_3^+ , $\text{FeCO}_3(\text{aq})$, and $\text{FeSO}_4(\text{aq})$. The dissolved Fe(II) in springs below pH 6.6 is mostly Fe^{2+} , while FeHCO_3^+ is found at 15–25% in this range. $\text{FeCO}_3(\text{aq})$ becomes abundant at pH 7 and above. Springs with relatively high concentrations of sulfate show minor concentrations of $\text{FeSO}_4(\text{aq})$. Other species, including $\text{Fe}(\text{CO}_3)_2^{2-}$, are present in amounts < 0.5% and can be found in the Supporting Information. The spring samples are as follows (from left to right): 150906C, 150907F, 150906B, 150908H, 150906D, 150911T, 150908J, 150907G, and 150905A. For spring designation see Table 1.

Table 6. Sediment Carbon, Iron, and Mineral Composition^a

sample ID	organic carbon, % ^b	$\delta^{13}\text{C}$ vPDB, ‰	total carbon, % ^b	$\delta^{13}\text{C}$ vPDB, ‰	Fe(II), dry wt %	Fe(III), dry wt %	sediment H_2O , mass %	minerals
150907F	0.12	−26.2	8.2	2.35	0.05	4.32 ± 0.2	32	dolomite, calcite, quartz
150908J	0.09	−28.2	11.3	7.89	0.12	1.24 ± 0.28	49	calcite
150907G	0.09	−24.0	11.5	8.83	0.05	0.33 ± 0.04	56	calcite
150906B	0.15	−27.6	5.7	2.14	0.3	13.53 ± 0.35	71	calcite
150906C	0.25	−23.4	2.7	−0.57	1.0	5.03 ± 1.04	75	quartz, calcite, clinochlore, illite
150908H	0.13	−23.9	5.0	1.51	0.25	2.11 ± 0.44	28	quartz, calcite
150905A	0.92	−29.5	8.0	6.94	0.18	1.98 ± 0.19	62	calcite, dolomite, quartz
150911T	0.12	−27.1	8.1	−0.07	0.12	0.35 ± 0.02	22	quartz, dolomite, calcite
150909K	2.47	−23.7	ND	ND	0.18	BDL	68	quartz, illite
150909L	0.53	−18.6	ND	ND	0.03	0.02 ± 0.02	26	quartz, albite
150909M	1.27	−22.8	ND	ND	0.01	0.02 ± 0.004	37	quartz, clinochlore, muscovite
150910O	0.37	−16.4	ND	ND	0.09	BDL	41	quartz, illite, clinochlore
150910Q	0.22	−14.7	ND	ND	0.01	BDL	21	quartz, illite, clinochlore
150910R	0.10	−18.1	ND	ND	0.01	0.01 ± 0.001	15	ND
150910S	0.58	−20.6	ND	ND	0.02	0.03 ± 0.001	37	ND

^aOrganic carbon measured by acidifying dry sediment samples to remove inorganic carbon. Organic carbon is generally indicative of microbial biomass in the system, with the exception of Arvadi, which had abundant plant organic matter in the sediment. Total carbon is measured on unacidified samples and contains organic and inorganic carbon. Minerals were identified by XRD. No iron minerals were identified despite often intense iron staining. Samples were frozen prior to analysis to minimize redox processes or other alteration. For sample designations see Tables 1 and 2. ND, not determined; BDL, below detection limit. ^bDry mass percent.

have significant total carbon contents as expected from XRD results, with values ranging from 2.7 to 11.5% C by dry weight. If the assumption is made that all of the inorganic C is carbonate, then carbonate makes up 14–57% of the total weight of the sediments.

Jöri lake sediments contain only quartz and other silicate minerals. The organic carbon content of the lake sediments ranges from 0.10 to 2.47%, which is considerably higher than that of the spring sediments. These lakes are situated several hundred meters above the tree line, with only sparse seasonal plants dotting the landscape. This implies that the source of organic carbon is largely from autotrophic biomass. The water column in lake XIII, with the highest organic sediment C, is dense with phototrophic biomass. The isotopic composition of the biomass C in the lakes is heavier than that in the iron springs. Total C measurements were not made in lake sediment samples because inorganic C was expected to be an insignificant component of the sediments.

3.3.2. Iron in Sediments. Ferric minerals are apparent in iron springs by red staining. The amount of iron present as ferric minerals was measured by reductive dissolutions with hydroxylamine and HCl, as well as Fe(II) in sediments determined by HCl extraction.³³ These iron values, along with water content of wet sediments, are shown in Table 6. All spring sediments at Alvaneu Bad and Val Sinestra showed relatively large concentrations of Fe(II). Given the strong drive toward oxidation, these relatively high values suggest biological reduction is occurring in the sediments. Sediments at Rablönch did not contain large concentrations of Fe(II). The amorphous ferric mineral content of all the springs ranged from 0.33 to 13.5% Fe by dry weight.

Lake sediments have much lower total iron concentrations. Lakes XIII and II, where iron oxidation was detected, have greater concentrations of Fe(II) in the sediments than the other lakes. Accumulations of Fe(II) in sediments suggest the presence of iron reducing microbes and is indicative of the source of Fe(II) for oxidation. The ferric mineral content of

the samples is below the detection limit of the reductive dissolution method, which is 0.0005 wt % Fe. Despite this lack of detection, a lightly stained 1 cm band of apparent ferric minerals was observed at 3 cm depth in lake II. Biological Fe(II) oxidation detected by experiment at this location (150910O) suggests this lake hosts complete microbial redox cycling. Other lakes in the area have relatively small sediment concentrations of Fe(II) and ferric minerals (Table 6) and are less redox active.

3.4. Study from Subsurface Geochemistry to Community Composition. Surface microbial community compositions reflect subsurface geochemistry and sediment processes. Isotope studies have revealed the source of water enriched in DIC that leads to the observed geochemical composition of springs in the region.^{54–56} Likewise, a study of metals in the Jöri lakes provides a framework for iron cycling based on a redox gradient in the sediments.⁵³ These studies set the background for linking the observed metabolic activity of the microbial communities to subsurface processes.

3.4.1. Subsurface Processes Control Fluid Composition. The isotopic composition of the water suggests extensive water–rock interaction in the source water of springs but meteoric water in the lakes. Stable isotopic composition of H and O in water of springs, lakes, and fresh water in the area are shown in Figure 7 (data in Table S23). Global and local meteoric water lines are included for reference. Note that the Jöri lakes' samples (black squares) fall close to these lines. The dilute nature of the lakes combined with the isotopic information support a conclusion that the lakes are composed of meteoric water with minimal water–rock interaction. This contrasts with most of the mineral springs (open squares), which show an oxygen enrichment, or a deuterium depletion, relative to both meteoric water lines. These isotopic compositions are interpreted to result from deep water–rock interactions.

The source of CO_2 in the springs of the lower Engadin region, which includes Rablönch and Val Sinestra, was

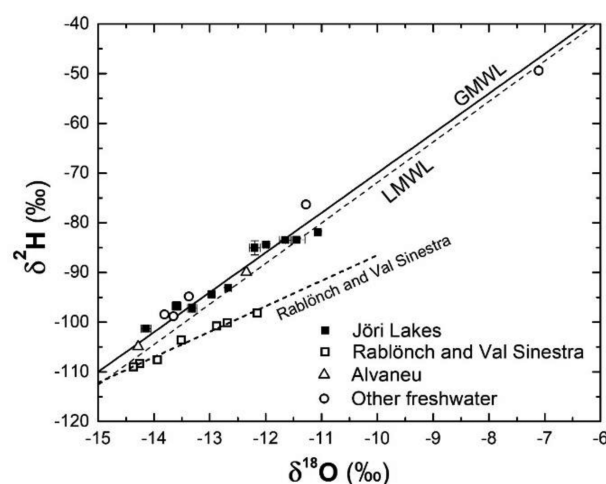


Figure 7. $\delta^2\text{H}$ vs $\delta^{18}\text{O}$ of all water samples collected in this study, including Jöri lakes (black squares), Rablönch and Val Sinestra (empty squares), Alvaneu Bad (empty triangles), and fresh water (circles) from the region (reported in per mil (‰) vs VSMOW). Fresh water samples include piled snow, creeks, rivers, and rain. The Global Meteoric Water Line (GMWL), as reported by Craig,⁵⁷ and a Local Meteoric Water Line (LMWL) reported by Strauss et al.⁵⁶ are included for reference. Samples from the Jöri lakes and Alvaneu are consistent with meteoric recharge. Many of the cold springs plot to the right of the LMWL, which can be caused by either an enrichment toward higher $^{18}\text{O}/^{16}\text{O}$ ratios or a depletion in ^2H , and are interpreted as resulting from water–rock interaction (see text). The thick dashed lined is the linear fit of Rablönch and Val Sinestra springs, with the equation $\delta^2\text{H} = 5.1 \delta^{18}\text{O} - 35.1$.

determined by Wexteen et al.⁵⁴ to ultimately arise from metamorphic reactions deep in the subsurface. In their model, the CO_2 rises and infiltrates a carbonate-rich aquifer, which results in DIC-rich water with high conductivity. They showed that dozens of mineral springs in the area can be grouped based on their anion and water isotope composition. Some springs fall close to the LMWL, but the most mineralized springs are enriched in ^{18}O . Evaporation could generate the observed $\delta^{18}\text{O}$ values, but this was determined to be unlikely due to current and past climate conditions in the region and conclude that water–rock reactions are the most plausible explanation for the observed $\delta^{18}\text{O}$ values.⁵⁴ These findings are consistent with our observations of higher concentrations of DIC (here a proxy for water–rock interaction) leading to depleted $\delta^{18}\text{O}$ values, as shown in Figure 8. Isotopic data reported by Strauss et al.⁵⁶ show less oxygen depletion for many samples from many of the same regional locations, inconsistent with the other studies and our data. Bissig et al.⁵⁵ constructed a conceptual model of groundwater and gas fluxes in the region, leading to the conclusion that there are two end-member sources of water: the DIC-rich aquifer and shallow groundwater. Rablönch and Val Sinestra area springs are composed predominantly of the deeper aquifer end-member fluid, rich in DIC and Fe(II). Consequently, these locations support the fastest rates of microbial Fe(II) oxidation and, as discussed next, contain the largest percentage of putative iron oxidizers.

3.4.2. Fluid Composition Control of Microbial Communities. Small subunit rRNA (16S rRNA) gene sequencing shows putative iron oxidizing bacteria are present in every system (data in Tables S24–S27). Archaeal iron oxidizing organisms were not identified. The dominant FeOB genus in almost every

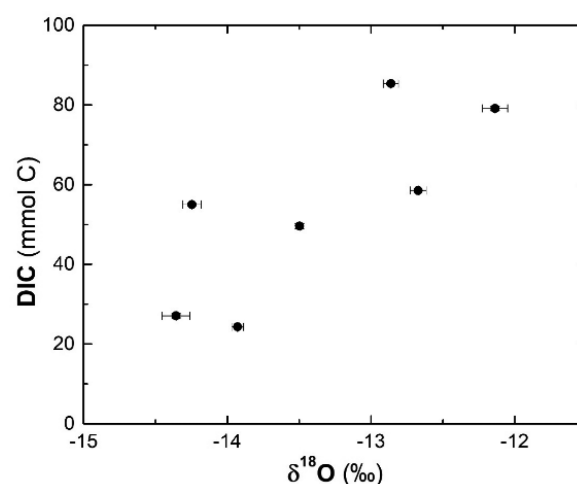


Figure 8. Concentration of dissolved inorganic carbon vs $\delta^{18}\text{O}$ (‰) of water in cold springs. The linear distribution of data is suggestive of subsurface water–rock interaction, most likely involving carbonate minerals.

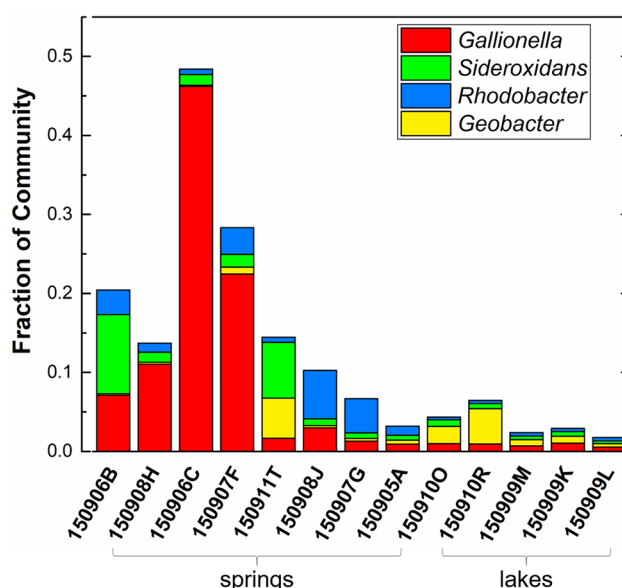


Figure 9. Microbial community, at the genus level, potentially involved in iron redox cycling in Swiss springs and lakes. Samples are arranged left to right from highest to lowest conductivity. All experimental locations are represented, in addition to contextual springs and lakes. Putative iron oxidizing genus *Gallionella* dominates the iron mats, while *Sideroxydans* are abundant in two locations. For sample designations see Tables 1 and 2

system is *Gallionella*, which ranges from 1.2 to 46% of the total community. The relative percentage of organisms putatively involved in iron redox metabolism are shown in Figure 9. Note that results in Figures 9 and 10 come from the Silva database. OTU abundances using the NCBI 16S rRNA database are similar, but not always identical, to results using the Silva database. Notably, some sequences identified as *Sideroxydans* by the NCBI database are identified as *Gallionella* by the Silva database. The data are presented in order of decreasing conductivity. In general, the higher the conductivity, which isotopic and geochemical data suggest is a proxy for water–rock interaction, the more putative iron oxidizers are present in the system. In addition to *Gallionella*, other putative FeOB

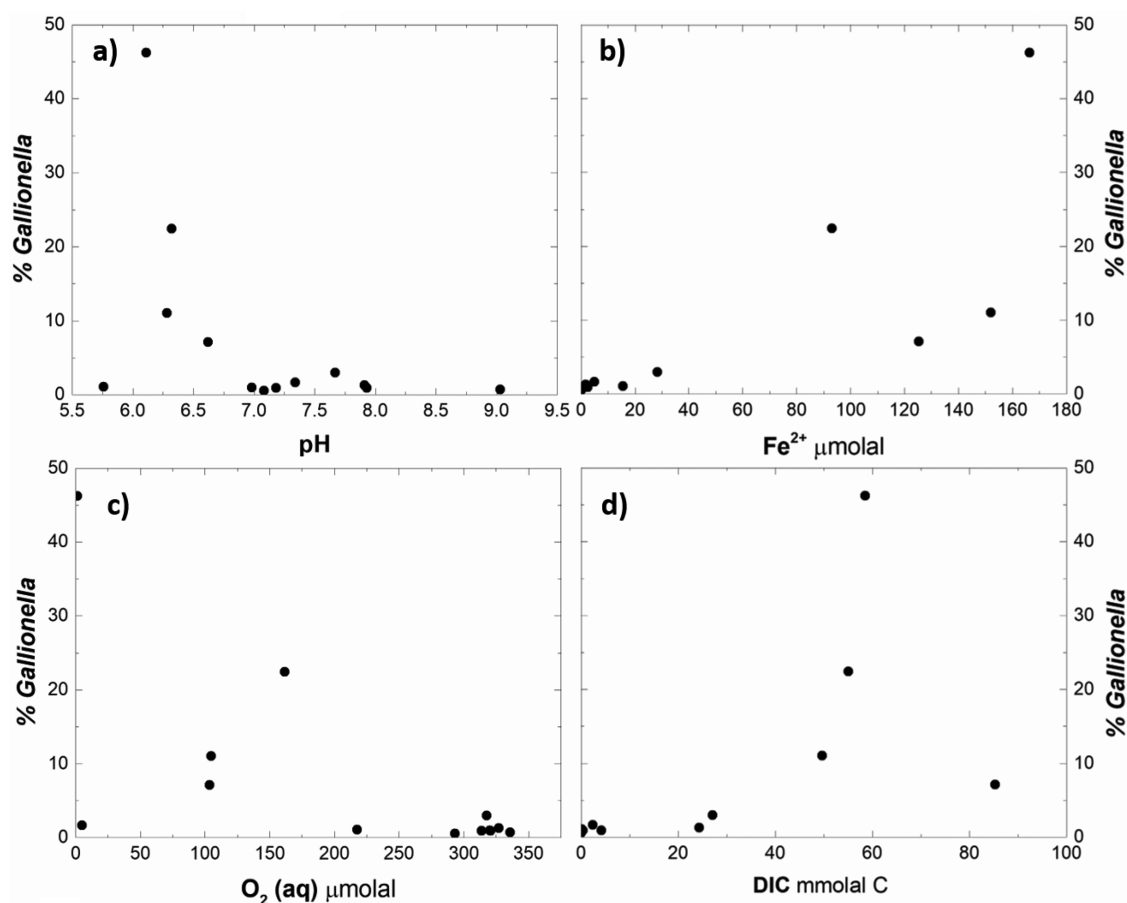


Figure 10. Presence of *Gallionella* in the sediment, as percent of total community, plotted against geochemical variables. *Gallionella* are most abundant between pH 6 and 7 (a), at concentrations of Fe(II) > 50 μM (b), and at bulk oxygen concentrations below $\sim 200 \mu\text{M}$ (c). Higher DIC concentrations also leading to higher abundances of *Gallionella* (d), possibly corresponding to increased water–rock reaction and correspondingly elevated concentrations of Fe(II).

genera present include *Sideroxydans* and *Rhodobacter* (photoferrotrophs). Yuhana et al.⁵⁷ also reported *Rhodoferrax* (photoferrotrophs) putative FeOB at Jori Lake XIII. Note that not all cultured representatives of these genera are known to oxidize iron.⁵⁸ The generally ubiquitous FeOB *Leptothrix* is poorly represented in all systems (<0.1%). *Geobacter* are a genera of metal reducing organisms often implicated in ferric mineral reduction. Significant numbers of these organisms were detected in several locations, notably a spring at Alvaneu (15911T) and most of Jori lake sites, which is strongly suggestive of coupled microbial iron oxidation and reduction. In comparison with the spring communities, lake samples show lower percentages of all putative FeOB. *Gallionella* are still the largest percentage of apparent FeOB in these systems, with a range between 0.74 and 1.35%. Further microbial community results can be found in section S5 of the Supporting Information.

The pH, O_2 , and Fe(II) niches of *Gallionella* and *Leptothrix* overlap, but the optima are not the same.¹⁵ Abundance of operational taxonomic units in the *Gallionella* genus as a percentage of the total community are shown in Figure 10 plotted against pH, ferrous iron, dissolved oxygen, and conductivity. *Gallionella* reached the largest percentages between pH 6.0 and 6.5 (Figure 10a), consistent with the optimum range of pH 6.3–6.6 described by Kucera and Wolfe.⁵⁹ In Figure 10b there is a positive trend of *Gallionella* percentage with Fe(II). Concentrations of Fe(II) higher than

100 μM lead to percentages between 7.5 and 46%. Bulk dissolved oxygen concentrations close to saturation appear to limit *Gallionella* (Figure 10c). The optimal dissolved oxygen range for *Gallionella* reported by Hanert⁶⁰ is 5.6–56 μM . Our findings show no apparent issues with *Gallionella* growing at O_2 concentrations as high as 160 μM . *Gallionella* are most abundant in locations with high DIC (Figure 10d), further implicating subsurface water–rock reaction in determining community composition. It should be noted that our data report geochemical composition of the water, and samples for sequencing consist of approximately the top centimeter of sediment. The actual geochemical concentrations experienced by the organisms could vary from our measurements. OTUs of the *Sideroxydans* genus plotted against the same geochemical data do not show clear geochemical niche differentiation. Like *Gallionella*, *Sideroxydans* have low abundance at $\text{O}_2 > 150 \mu\text{M}$ (see Figure S16 in the Supporting Information). It is unclear what causes the nearly complete absence of *Leptothrix* OTU sequences, given that, for the range of pH, Fe(II) and O_2 have been found to support this putative FeOB. Fleming et al.⁶¹ identified low dissolved organic carbon as a primary determinant of ecological niche of *Gallionella*, while *Leptothrix* thrive in high DOC, high Fe(II)/Mn(II) environments. As discussed above, all sample sites in this study have low concentrations of DOC, with the highest concentration reaching only 141 μM C, which may limit *Leptothrix*. Efforts were made in this study to measure formate, acetate, lactate,

and propionate but showed that these organic acids were all close to or below the detection limit (~ 10 ppb), as documented in Table S22 in the Supporting Information.

3.4.3. Microenvironments. Many authors have recognized that FeOB must compete for available Fe(II) with the rapid abiotic oxidation rate.^{4,14,16,62} Here we have characterized rates in 10 geochemically variable systems to determine conditions that favor microbial oxidation and conditions where the abiotic iron oxidation rate excludes the biotic process. Cold systems with high concentrations of DIC appear to support microbial Fe(II) oxidation below pH values of 7.4. While this does not definitely exclude biological oxidation at higher pH values in this temperature range, it does indicate that biological Fe(II) oxidation is not a major contributor to the bulk iron oxidation rate at high pH. It is possible that FeOB occur in microenvironments or oxidize iron at rates below the detection limits of the experiments. Indeed, Koeksoy et al.⁶³ used most probably number counts to determine that a small community of FeOB inhabit Arvadi spring, a location featuring rapid abiotic Fe(II) oxidation where our method did not detect a biological signal. In most experiments, the difference in the rate of biological and abiotic oxidation must be greater than $0.1 \mu\text{M}/\text{min}$ for the standard protocol or $0.05 \mu\text{M}/\text{min}$ for the modified protocol to determine that biology is enhancing the rate. Given that these are natural systems that experience unknown compositional variability throughout the year and that experiments are being done in remote locations, the threshold for determining that biology is a major contributor to the rate varies slightly among experiments.

Microenvironments of elevated Fe(II) and low levels of oxygen that exist in layers buried in iron mats may extend the pH range of FeOB greater than that observable by microcosm experiments with bulk sediment and water. Microbial iron reduction almost invariably accompanies iron oxidation.^{64–66} Biological reduction of the biogenic ferric minerals within iron mats may permit low numbers of FeOB in systems where a biological rate was not detected. Our reported values of Fe(II) were sampled in the water right above the mat, but sediments at many locations showed higher concentrations of Fe(II) (Table 6). Our sequencing results often show low abundances of putative metal reducers such as *Geobacter*. Indeed, Hegler et al.⁵ determined that iron reduction was happening in situ at an iron mat very compositionally similar (and geographically close) to that of Rablönch. Sequencing results and visibly apparent photosynthesis imply local oxygen concentrations may also vary significantly from bulk values. The decay of organic matter in the mats may also allow for chelated ferrous ions to persist and extend their bioavailable tenure. Given these caveats, biological iron oxidation may well occur at pH values greater than those detected during our experiments, but it is unlikely to be a significant biogeochemical process.

4. CONCLUDING REMARKS

Microbial Fe(II) oxidation has long been known to compete with rapid abiotic oxidation in cold circumneutral systems. However, as shown in this study, there are conditions where the abiotic reaction is too fast for biology to compete. Microcosm experiments reported here provide biotic and abiotic oxidation rates at a variety of pH and other conditions and reveal geochemical conditions that exclude microbial iron oxidation. In these cold ($8\text{--}12^\circ\text{C}$), circumneutral systems, biological iron oxidation was only detected up to pH 7.4. Comparing relative biotic and abiotic rates suggests that the

maximum pH for biological Fe(II) oxidation of any biogeochemical significance at the conditions studied is around 7.5. At higher pH values, ferrous iron is oxidatively precipitated within seconds by abiotic processes, rendering it unavailable to FeOB. This was determined to be the case in both the dilute Jöri lake systems and the iron-rich springs. The underlying cause for the expedited abiotic rate is the change in speciation of Fe(II) in solution. More reactive aqueous species form at higher pH values, especially the (bi)carbonate complexes that form in the presence of dissolved inorganic carbon, as revealed by new thermodynamic estimates. In systems with different compositions than those reported here, such as locations lacking bicarbonate or with abundant Fe(II)-stabilizing organic compounds, alternate Fe(II) speciation may slightly alter the pH values at which exclusively abiotic oxidation is observed. FeOB make up a small percentage of the community in the Jöri lakes, while they are dominant in the springs. The iron oxidizing microbial communities are composed predominantly of the genus *Gallionella*. The abundance of *Gallionella* in each system depends on oxygen, Fe(II), and pH and largely agrees with published data on geochemical niches of the genus. Taken together, these data yield an inventory of magnitudes of biotic and abiotic oxidation transformations of iron in these systems, provide a geochemical explanation for the observed rates, and describe the communities that oxidize Fe(II).

The kinetic challenge faced by iron oxidizing microbes in circumneutral environments undoubtedly extends to all temperatures where Fe(II) oxidation is physiologically possible. Circumneutral iron oxidation has been studied extensively at low temperatures, but reports from higher temperature are scarce. Rate measurements in such systems are non-existent. This is, in part, due to the fact that the iron-rich circumneutral systems at elevated temperatures are uncommon. Iron oxidizing microbes have been isolated from mesophilic⁶⁷ and thermophilic⁶⁸ acidic systems. It is likely that Fe(II) oxidizing microbes also inhabit circumneutral environments at higher temperatures. Abiotic rates in such systems are undoubtedly also dictated by pH and chemical speciation. This implies there is a continuous boundary to the habitability of the iron oxidation reaction in pH and temperature space that is determined by the rate at which biology cannot compete. Extreme kinetic dissipation rates exist for numerous other solutes at conditions common on Earth's surface. Quantification of these rates relative to the rate catalyzed by the microbial community can inform discussions of the contribution of these reactions to habitability on Earth and beyond.

■ ASSOCIATED CONTENT

● Supporting Information

The Supporting Information is available free of charge on the ACS Publications website at DOI: 10.1021/acsearthspacechem.9b00016.

Detailed summary of thermodynamic data and methods used in speciation calculations (section S1), an extended site description (maps and compositional data, section S2), complete rate experiment data (section S3), geochemical data (section S4), and detailed phylogenetic data (section S5) (PDF)

AUTHOR INFORMATION

Corresponding Author

*E-mail: bstclair@mtech.edu (Montana address).

ORCID

Brian St Clair: 0000-0002-5843-0754

Present Address

#CDepartment of Chemistry and Geochemistry, Montana Technological University, 1300 W Park St., Butte, MT 59701.

Funding

This work was funded by the National Science Foundation (Grant EAR-1529963).

Notes

The authors declare no competing financial interest.

ACKNOWLEDGMENTS

Many people share credit for the development and refinement of the field and analytical methods used in this work. Kris Fecteau performed the ion chromatography analyses. Grayson Boyer and Natasha Zolotova helped analyze DIC, DOC, and sediment C on the IRMS. Eric Boyd, Melody Lindsay, and Dan Coleman at Montana State University provided laboratory space and guidance for the molecular biology work. Cody Sheik performed 16s OTU alignments with Mothur. This work could also not have been done without logistical assistance in Switzerland. Daniel Montluçon at ETH Zurich helped us obtain compressed gas and chemicals prohibited by commercial air travel, as well as provided laboratory space to prepare reagents. Alysia Cox helped collect samples during the preliminary sampling trip in 2012.

REFERENCES

- (1) Straub, K. L.; Benz, M.; Schink, B.; Widdel, F. Anaerobic, nitrate-dependent microbial oxidation of ferrous iron. *Appl. Environ. Microbiol.* **1996**, *62*, 1458–1460.
- (2) Widdel, F.; Ehrenreich, A.; Heising, S.; Schnell, S.; Assmus, B.; Schink, B. Ferrous iron oxidation by anoxygenic phototrophic bacteria. *Nature* **1993**, *362*, 834–836.
- (3) Dubinina, G.; Sorokina, A. Neutrophilic lithotrophic iron-oxidizing prokaryotes and their role in the biogeochemical processes of the iron cycle. *Microbiology* **2014**, *83*, 1–14.
- (4) James, R.; Ferris, F. Evidence for microbial-mediated iron oxidation at a neutrophilic groundwater spring. *Chem. Geol.* **2004**, *212*, 301–311.
- (5) Hegler, D.; Lösekann-Behrens, T.; Hanselmann, K.; Behrens, S.; Kappler, A. Influence of seasonal and geochemical changes on the geomicrobiology of an iron carbonate mineral water spring. *Appl. Environ. Microbiol.* **2012**, *78*, 7185–7196.
- (6) Emerson, D.; Scott, J.; Benes, J.; Bowden, W. Microbial iron oxidation in the Arctic tundra and its implications for biogeochemical cycling. *Appl. Environ. Microbiol.* **2015**, *81*, 8066.
- (7) Kasama, T.; Murakami, T. The effect of microorganisms on Fe precipitation rates at neutral pH. *Chem. Geol.* **2001**, *180*, 117–128.
- (8) McAllister, S.; Davis, R.; McBeth, J.; Tebo, B.; Emerson, D.; Moyer, C. Biodiversity and emerging biogeography of the neutrophilic iron-oxidizing zeta-proteobacteria. *Appl. Environ. Microbiol.* **2011**, *77*, 5445–5457.
- (9) Rentz, J.; Kraiya, C.; Luther, G.; Emerson, D. Control of ferrous iron oxidation within circumneutral microbial iron mats by cellular activity and autocatalysis. *Environ. Sci. Technol.* **2007**, *41*, 6084–6089.
- (10) Ferris, F.; Enright, A.; Fortin, D.; Clark, I. Rates of Fe(II)-oxidation and solubility of bacteriogenic iron oxides. *Geomicrobiol. J.* **2016**, *33*, 237–242.
- (11) Emerson, D.; Fleming, E.; McBeth, J. Iron-oxidizing bacteria: an environmental and genomic perspective. *Annu. Rev. Microbiol.* **2010**, *64*, 561–583.
- (12) Neubauer, S.; Emerson, D.; Megonigal, J. Life at the energetic edge: kinetics of circumneutral iron oxidation by lithotrophic iron-oxidizing bacteria isolated from the wetland-plant rhizosphere. *Appl. Environ. Microbiol.* **2002**, *68*, 3988–3995.
- (13) Sobolev, D.; Roden, E. Characterization of a neutrophilic, chemolithoautotrophic Fe(II)-oxidizing β -proteobacterium from freshwater wetland sediments. *Geomicrobiol. J.* **2004**, *21*, 1–10.
- (14) Druschel, G.; Emerson, D.; Sutka, R.; Suchecki, P.; Luther, G. Low-oxygen and chemical kinetic constraints on the geochemical niche of neutrophilic iron(II) oxidizing microorganisms. *Geochim. Cosmochim. Acta* **2008**, *72*, 3358–3370.
- (15) Eggerichs, T.; Opel, O.; Otte, T.; Ruck, W. Interdependencies between biotic and abiotic ferrous iron oxidation and influence of pH, oxygen and ferric iron deposits. *Geomicrobiol. J.* **2014**, *31*, 461–472.
- (16) Melton, E.; Swanner, E.; Behrens, S.; Schmidt, C.; Kappler, A. The interplay of microbially mediated and abiotic reactions in the biogeochemical Fe cycle. *Nat. Rev. Microbiol.* **2014**, *12*, 797–808.
- (17) Stumm, W.; Lee, G. (1961) Oxygenation of ferrous iron. *Ind. Eng. Chem.* **1961**, *53*, 143–146.
- (18) Lowson, R. Aqueous oxidation of pyrite by molecular oxygen. *Chem. Rev.* **1982**, *82*, 461–497.
- (19) Millero, F. The effect of ionic interactions on the oxidation of metals in natural waters. *Geochim. Cosmochim. Acta* **1985**, *49*, 547–553.
- (20) Morgan, B.; Lahav, O. The effect of pH on the kinetics of spontaneous Fe(II) oxidation by O₂ in aqueous solution—basic principles and a simple heuristic description. *Chemosphere* **2007**, *68*, 2080–2084.
- (21) Millero, F.; Izaguirre, M. Effect of ionic strength and ionic interactions on the oxidation of Fe(II). *J. Solution Chem.* **1989**, *18*, 585–599.
- (22) Santana-Casiano, J. M.; Gonzalez-Davila, M. J.; Rodriguez, M.; Millero, F. The effect of organic compounds in the oxidation kinetics of Fe(II). *Mar. Chem.* **2000**, *70*, 211–222.
- (23) Park, U.; Dempsey, B. Heterogeneous oxidation of Fe(II) on ferric oxide at neutral pH and a low partial pressure of O₂. *Environ. Sci. Technol.* **2005**, *39*, 6494–6500.
- (24) Millero, F.; Yao, W.; Aicher, J. The speciation of Fe(II) and Fe(III) in natural waters. *Mar. Chem.* **1995**, *50*, 21–39.
- (25) Bruno, J.; Wersin, P.; Stumm, W. On the influence of carbonate in mineral dissolution: II. The solubility of FeCO₃(s) at 25°C and 1 atm total pressure. *Geochim. Cosmochim. Acta* **1992**, *56*, 1149–1155.
- (26) King, D. Role of carbonate speciation on the oxidation rate of Fe(II) in aquatic systems. *Environ. Sci. Technol.* **1998**, *32*, 2997–3003.
- (27) Fosbøl, P.; Thomsen, K.; Stenby, E. Review and recommended thermodynamic properties of FeCO₃. *Corros. Eng., Sci. Technol.* **2010**, *45*, 115–135.
- (28) Lemire, R. J.; Berner, U.; Musikas, C.; Palmer, D. A.; Taylor, P.; Tochiyama, O. (2013) *Chemical Thermodynamics of Iron, Part 1*; OECD publications, Paris. 13a. 1082.
- (29) Meyer-Dombard, D. R.; Woycheese, K. M.; Yargıçoğlu, E. N.; Cardace, D.; Shock, E. L.; Güleç-Pektas, Y.; Temel, M. High pH microbial ecosystems in a newly discovered, ephemeral, serpentinizing fluid seep at Yanartaş (Chimera), Turkey. *Front. Microbiol.* **2015**, *5*, 723.
- (30) Havig, J.; Raymond, J.; Meyer-Dombard, D.; Zolotova, N.; Shock, E. Merging isotopes and community genomics in a siliceous sinter-depositing hot spring. *J. Geophys. Res.* **2011**, *116*, G01005.
- (31) Schubotz, F.; Meyer-Dombard, D.; Bradley, A.; Fredricks, H.; Hinrichs, K.; Shock, E.; Summons, R. Spatial and temporal variability of biomarkers and microbial diversity reveal metabolic and community flexibility in Streamer Biofilm Communities in the Lower Geyser Basin, Yellowstone National Park. *Geobio.* **2013**, *11*, 549–569.
- (32) Canovas, P.; Hoehler, T.; Shock, E. Geochemical bioenergetics during low-temperature serpentinization: An example from the Samail

ophiolite, Sultanate of Oman. *J. Geophys. Res.: Biogeosci.* **2017**, *122*, 1821–1847.

(33) Lovely, D.; Phillips, E. Rapid assay for microbially reducible ferric iron in aquatic sediments. *Appl. Environ. Microbiol.* **1987**, *53*, 1536–1540.

(34) Stookey, L. Ferrozine - A new spectrophotometric reagent for iron. *Anal. Chem.* **1970**, *42*, 779–781.

(35) Colman, D. R.; Feyhl-Buska, J.; Fecteau, K. M.; Xu, H.; Shock, E. L.; Boyd, E. S.; Robinson, K. J. Ecological differentiation in planktonic and sediment-associated chemotrophic microbial populations in Yellowstone hot springs. *FEMS Microbiol. Ecol.* **2016**, *92*, fiw137.

(36) Schloss, P. D.; Westcott, S. L.; Ryabin, T.; Hall, J. R.; Hartmann, M.; Hollister, E. B.; Lesniewski, R. A.; Oakley, B. B.; Parks, D. H.; Robinson, C. J.; Sahl, J. W.; Stres, B.; Thallinger, G. G.; Van Horn, D. J.; Weber, C. F. Introducing mothur: Open-source, platform independent, community-supported software for describing and comparing microbial communities. *Appl. Environ. Microbiol.* **2009**, *75*, 7537–7541.

(37) Hamilton, T.; Peters, J.; Skidmore, M.; Boyd, E. Molecular evidence for an active endogenous microbiome beneath glacial ice. *ISME J.* **2013**, *7*, 1402.

(38) Quast, C.; Pruesse, E.; Gerken, J.; Peplies, J.; Yarza, P.; Yilmaz, P.; Schweer, T.; Glöckner, F. The SILVA ribosomal RNA gene database project: improved data processing and web-based tools. *Nucleic Acids Res.* **2012**, *41*, D590–D596.

(39) Yilmaz, P.; Pruesse, E.; Gerken, J.; Quast, C.; Peplies, J.; Parfrey, L. W.; Yarza, P.; Schweer, T.; Ludwig, W.; Glöckner, F. O. The SILVA and “All-species Living Tree Project (LTP)” taxonomic frameworks. *Nucleic Acids Res.* **2014**, *42*, D643–D648.

(40) Wolery, T.; Jarek, R. *Software User's Manual EQ3/6, Version 8.0*, Development Software Document No. 10813-UM-8.0-00; Office of Civilian Radioactive Waste Management, Office of Repository Development, U.S. Department of Energy: Las Vegas, NV, USA, 2003.

(41) Helgeson, H.; Delany, J.; Nesbitt, H.; Bird, D. Summary and critique of the thermodynamic properties of rock-forming minerals. *Am. J. Sci.* **1978**, *278A*, 1–229.

(42) Shock, E.; Helgeson, H.; Sverjensky, D. Calculation of the thermodynamic and transport properties of aqueous species at high pressures and temperatures: standard partial molal properties of inorganic neutral species. *Geochim. Cosmochim. Acta* **1989**, *53*, 2157–2183.

(43) Shock, E.; Sassani, D.; Willis, M.; Sverjensky, D. Inorganic species in geologic fluids: Correlations among standard molal thermodynamic properties of aqueous ions and hydroxide complexes. *Geochim. Cosmochim. Acta* **1997**, *61*, 907–950.

(44) Shock, E.; McKinnon, W. Hydrothermal processing of cometary volatiles-applications to Triton. *Icarus* **1993**, *106*, 464–477.

(45) Sverjensky, D.; Shock, E.; Helgeson, H. Prediction of the thermodynamic properties of aqueous metal complexes to 1000 °C and 5 kb. *Geochim. Cosmochim. Acta* **1997**, *61*, 1359–1412.

(46) Shock, E. Minerals as energy sources for microorganisms. *Econ. Geol. Bull. Soc. Econ. Geol.* **2009**, *104*, 1235–1248.

(47) Shock, E.; Helgeson, H. Calculation of the thermodynamic and transport properties of aqueous species at high pressures and temperatures: Correlation algorithms for ionic species and equation of state predictions to 5 kb and 1000°C. *Geochim. Cosmochim. Acta* **1988**, *52*, 2009–2036.

(48) Shock, E.; Koretsky, C. Metal-organic complexes in geochemical processes: Estimation of standard partial molal thermodynamic properties of aqueous complexes between metal cations and monovalent organic acid ligands at high pressures and temperatures. *Geochim. Cosmochim. Acta* **1995**, *59*, 1497–1532.

(49) Murphy, W.; Shock, E. Environmental aqueous geochemistry of actinides. *Rev. Mineral.* **1999**, *38*, 221–253.

(50) Shock, E.; Oelkers, E.; Johnson, J.; Sverjensky, D.; Helgeson, H. V. Calculation of the thermodynamic properties of aqueous species at high pressures and temperatures. Effective electrostatic radii,

dissociation constants and standard partial molal properties to 1000 C and 5 kbar. *J. Chem. Soc., Faraday Trans.* **1992**, *88*, 803.

(51) Dick, J. Calculation of the relative metastabilities of proteins using the CHNOSZ software package. *Geochem. Trans.* **2008**, *9*, 1–17.

(52) Helgeson, H. Thermodynamics of hydrothermal systems at elevated temperatures and pressures. *Am. J. Sci.* **1969**, *267*, 729–804.

(53) Steiner, B.; Hanselmann, K.; Krähenbühl, U. Dating and heavy metal contents of sediment cores of a high-alpine, remote lake: Jörisee (Switzerland). *Int. J. Environ. Anal. Chem.* **2000**, *78*, 131–148.

(54) Wexsteen, P.; Jaffé, F.; Mazor, M. Geochemistry of cold CO₂-rich springs of the Scuol-Tarasp region, Lower Engadine, Swiss Alps. *J. Hydrol.* **1988**, *104*, 77–92.

(55) Bissig, P.; Goldscheider, N.; Mayoraz, J.; Surbeck, H.; Vuataz, F. Carbogaseous spring waters, coldwater geysers and dry CO₂ exhalations in the tectonic window of the Lower Engadine Valley, Switzerland. *Eclogae Geol. Helv.* **2006**, *99*, 143–155.

(56) Strauss, H.; Chmiel, H.; Christ, A.; Fugmann, A.; Hanselmann, K.; Kappler, A.; Königer, P.; Lutter, A.; Siedenberg, K.; Teichert, B. Multiple sulphur and oxygen isotopes reveal microbial sulphur cycling in spring waters in the Lower Engadin, Switzerland. *Isot. Environ. Health Stud.* **2016**, *52*, 75–93.

(57) Craig, H. Isotopic variations in meteoric waters. *Science* **1961**, *133*, 1702–1703.

(58) Yuhana, M.; Horath, T.; Hanselmann, K. Bacterial community shifts of a high mountain lake in response to variable simulated conditions: availability of nutrients, light and oxygen. *Biotropia* **2006**, *13*, 85–98.

(59) Kucera, S.; Wolfe, R. A selective enrichment method for *Gallionella ferruginea*. *J. Bacteriol.* **1957**, *74*, 344–349.

(60) Hanert, H. The Genus *Gallionella*. In *The Prokaryotes*; Dworkin, M., Falkow, S., Rosenberg, E., Schleifer, K. H., Stackebrandt, E., Eds.; Springer: New York, NY, USA, 2006; pp 990–995.

(61) Fleming, E.; Cetinić, I.; Chan, C.; Whitney King, D.; Emerson, D. Ecological succession among iron-oxidizing bacteria. *ISME J.* **2014**, *v8*, 804–815.

(62) Emerson, D.; Moyer, C. Isolation and characterization of novel iron-oxidizing bacteria that grow at circumneutral pH. *Appl. Environ. Microbiol.* **1997**, *63*, 4784–4792.

(63) Koeksoy, E.; Halama, M.; Hagemann, N.; Weigold, P.; Laufer, K.; Kleindienst, S.; Byrne, J. M.; Sundman, A.; Hanselmann, K.; Halevy, I.; Schoenberg, R.; Konhauser, K.; Kappler, A. A case study for late Archean and Proterozoic biogeochemical iron- and sulphur cycling in a modern habitat—the Arvadi Spring. *Geobio.* **2018**, *16*, 353–368.

(64) Blöthe, M.; Roden, E. Microbial iron redox cycling in a circumneutral-pH groundwater seep. *Appl. Environ. Microbiol.* **2009**, *75*, 468–473.

(65) Roden, E. Microbial iron-redox cycling in subsurface environments. *Biochem. Soc. Trans.* **2012**, *40*, 1249–1256.

(66) Ionescu, D.; Heim, C.; Polerecky, L.; Thiel, V.; de Beer, D. Biotic and abiotic oxidation and reduction of iron at circumneutral pH are inseparable processes under natural conditions. *Geomicrobiol. J.* **2015**, *32*, 221–230.

(67) Clark, D.; Norris, P. *Acidimicrobium ferrooxidans* gen. nov., sp. nov.: mixed-culture ferrous iron oxidation with *Sulfobacillus* species. *Microbiology* **1996**, *142*, 785–790.

(68) Kozubal, M.; Macur, R.; Korf, S.; Taylor, W.; Ackerman, G.; Nagy, A.; Inskeep, W. Isolation and distribution of a novel iron-oxidizing crenarchaeon from acidic geothermal springs in Yellowstone National Park. *Appl. Environ. Microbiol.* **2008**, *74*, 942–949.